Geochemistry, U–Pb Geochronology and Genesis of Granitoid Clasts in Transported VMS Ore Deposits, Buchans, Newfoundland

Article *in* Canadian Journal of Earth Sciences · August 2013

DOI: 10.1139/cjes-2013-0040

4 authors:

Joseph B Whalen
Natural Resources Canada
122 PUBLICATIONS **3,955** CITATIONS
SEE PROFILE

Alexandre Zagorevski
Natural Resources Canada
44 PUBLICATIONS **663** CITATIONS
SEE PROFILE

Vicki Mcnicoll
Natural Resources Canada
137 PUBLICATIONS **1,742** CITATIONS
SEE PROFILE

Neil Rogers
Government of Canada
35 PUBLICATIONS **549** CITATIONS
SEE PROFILE

NRC Research Press

ARTICLE

Geochemistry, U–Pb geochronology, and genesis of granitoid clasts in transported volcanogenic massive sulfide ore deposits, Buchans, Newfoundland[1]

J.B. Whalen, A. Zagorevski, V.J. McNicoll, and N. Rogers

Abstract: The Buchans Group, central Newfoundland, represents an Ordovician continental bimodal calc-alkaline arc sequence that hosts numerous volcanogenic massive sulfide (VMS) occurrences, including both in situ and mechanically transported sulfide breccia–conglomerate orebodies. Diverse lithic clasts associated with transported deposits include rounded granitoid clasts. Earlier workers have suggested that Buchans Group VMS-hosting felsic extrusive units, small granodiorite intrusions (e.g., Wiley's Brook), and granitoid cobbles associated with transported ore represent co-genetic products of the same magmatic system. The granitoid cobbles and small granodiorite intrusions are geochemically similar and closely resemble Buchans Group felsic volcanic units. U–Pb zircon age determinations show a (*i*) 466.7 ± 0.5 Ma crystallization age for the Wiley's Brook granodiorite (WBG), (*ii*) 464 ± 4 Ma crystallization age for a granitoid cobble, and (*iii*) 466 ± 4 Ma maximum deposition age for a conglomerate–sandstone sequence associated with transported ore. Thus, Buchans Group felsic plutonic rocks are within experimental error of felsic volcanism and VMS deposition. Furthermore, ε_{Nd} (*T*) (*T*, time of crystallization) values of four granitoid cobbles (–1.95 to –4.0) overlap values obtained from Buchans Group felsic volcanic units. Our results are compatible with plutonic and volcanic rocks being related through fractional crystallization or partial melting processes but do not support a petrogenetic link between VMS deposition and exposed felsic plutons. Comparisons to modern arc analogues favour exhumation of plutonic rocks by extension along caldera or rift walls and (or) subaerial erosion. Enigmatic rounding of Buchans granitoid clasts was likely accomplished in a subaerial or shallow marine environment, and the clasts transported into a VMS-active basin by mass flows.

Résumé : Le Groupe de Buchans, du centre de Terre-Neuve, représente une séquence calco-alcaline, bimodale, d'arc continental, datant de l'Ordovicien, contenant de nombreux amas de sulfures massifs volcanogènes (SMV), lesquels comprennent des zones de minéralisations de sulfures dans des brèches-conglomérats, in situ et transportées mécaniquement. Divers clastes lithiques associés aux gisements transportés comprennent des clastes granitoïdes arrondis. D'autres chercheurs ont antérieurement suggéré que les unités extrusives felsiques, contenant les SMV du Groupe de Buchans, de petites intrusions de granodiorite (p. ex. Wiley's Brook) et des cailloux granitoïdes associés au minerai transporté, représentent des produits cogénétiques du même système magmatique. Les cailloux granitoïdes et les petites inclusions de granodiorite sont géochimiquement similaires et ressemblent étroitement aux unités volcaniques felsiques du Groupe de Buchans. Des déterminations d'âge U–Pb sur zircon montrent : (*i*) une cristallisation à 466,7 ± 0,5 Ma pour la granodiorite de Wiley's Brook; (*ii*) une cristallisation à 464 ± 4 Ma pour un caillou granitoïde et (*iii*) un âge de déposition maximum de 466 ± 4 Ma pour une séquence de conglomérat-grès associée au minerai transporté. Les roches plutoniques felsiques du Groupe de Buchans se trouvent ainsi à l'intérieur de l'erreur expérimentale du volcanisme felsique et de la déposition des SMV. De plus, les valeurs ε_{Nd} (*T*) de quatre cailloux granitoïdes (–1,95 à –4,0) chevauchent des valeurs obtenues des unités volcaniques felsiques du Groupe de Buchans. Nos résultats concordent avec une relation, par cristallisation fractionnelle, entre les roches plutoniques et volcaniques, ou un processus de fusion partiel, mais ils ne supportent pas un lien pétrogénétique entre la déposition des SMV et les plutons felsiques affleurant. Des comparaisons avec des arcs modernes analogues favorisent une exhumation de roches plutoniques par extension le long de la caldera/ des murs de la distension et/ou par érosion subaérienne. L'arrondissement énigmatique des clastes granitoïdes de Buchans s'est probablement produit dans un environnement subaérien ou marin peu profond et les clastes auraient été transportés par des écoulements de masse dans un bassin de SMV actif. [Traduit par la Rédaction]

Introduction

The Buchans area of central Newfoundland is underlain by volcanic, sedimentary, and plutonic rocks that formed on the Laurentian margin owing to Ordovician to Silurian closure of Iapetus Ocean and its marginal basins (van Staal et al. 1998, 2007). Volcanogenic massive sulfide (VMS) deposits at Buchans occur as three genetically related types: stockwork ore, in situ ore, and mechanically transported fragmental ore (Thurlow 1981*b*; Thurlow and Swanson 1981). These orebodies are thought to have formed in a fashion analogous to the Tertiary Kuroko deposits of Japan (Thurlow 1977, 1981*a*, 1981*b*). The transported ore consists of a series of sulfide-bearing breccia–conglomerate beds containing diverse lithic clasts, including plutonic rocks of felsic to intermediate composition (granitoids) within a subaqueous sequence of volcanic, volcaniclastic, and sedimentary rocks. Thurlow (1981*b*) suggested that the mechanically transported granitoid cobbles, small felsic intrusions exposed both in Wiley's Brook and at Little

Received 21 March 2013. Accepted 9 July 2013.

Paper handled by Associate Editor Fernando Corfu.

J.B. Whalen, A. Zagorevski, V.J. McNicoll, and N. Rogers. Geological Survey of Canada, 601 Booth Street, Ottawa, ON K1A 0E8, Canada.
Corresponding author: Joseph Whalen (email: jwhalen@NRCan.gc.ca).

[1]Geological Survey of Canada (GSC) Contribution 20130171.

Sandy Lake near Buchans (termed Feeder Granodiorite), and Buchans Group felsic extrusive rocks were co-magmatic. Subsequently, Stewart (1984, 1985, and 1987) undertook a detailed study of the granitoid cobbles to investigate their petrology, geochemistry, and genetic relationship to other felsic magmatism within the Buchans camp.

Since this 1980s work, significant progress has been made in the tectonic and geodynamic understanding of central Newfoundland (e.g., van Staal et al. 1998, 2007; Zagorevski et al. 2006, 2009, 2010; Lissenberg et al. 2005; Whalen et al. 1997, 2006), and improved trace-element, tracer-isotope, and U–Pb zircon analytical techniques are available to evaluate postulated co-magmatic relationships within the Buchans camp (cf., Thurlow 1981*b*). The intent of this study is to revise, based on new geochronological, geochemical, and Nd isotopic analyses, the genesis of the transported, ore-hosted granitoid cobbles at Buchans and to place them within an updated local and regional tectonomagmatic context.

Geological context

The Buchans Group is a continental bimodal calc-alkaline arc sequence (Thurlow and Swanson 1987; Swinden et al. 1997) that hosts numerous VMS occurrences. It consists of imbricated belts composed primarily of bimodal arc volcanic rocks, the structural base of which exposes small high-level plutonic rocks (e.g., Wiley's Brook granodiorite (WBG), this study). Collectively these rocks form part of the Annieopsquotch accretionary tract (AAT), which consists of various supra-subduction zone ophiolite, arc, and back-arc terranes that were sequentially accreted to the composite Laurentian margin during the polyphase Middle Ordovician Taconic Orogeny (Zagorevski et al. 2009 and references therein) (Fig. 1). Although formed in the same arc system, these terranes exhibit differences in age, stratigraphy, chemistry, and basement characteristics, indicating that they represent distinct parts of the arc, back-arc, and remnant arc (Zagorevski et al. 2009).

The complex structural history, similar petrographic appearance, and along-strike variation in volcano-sedimentary facies within the Buchans area hamper correlations outside of the mineralized, fault-bound blocks that host the Oriental and MacLean orebodies in which the mine-scale stratigraphy was established. Application of geochemistry and new U–Pb zircon geochronology to the petrographically similar units has revealed significant differences between the type locality of the Buchans Group and sequences in adjacent structural panels, thus requiring their exclusion from the Buchans Group (e.g., Zagorevski et al. 2006, 2010; Zagorevski and Rogers 2008, 2009). A new framework for the Buchans area divides it into several arc-related tectonostratigraphic units, and an overlap sequence within which mineralized and barren sequences can be interpreted on a regional scale beyond the historic mining camp. Paleontological constraints (Nowlan and Thurlow 1984) and radiometric dating (U–Pb zircon) of units within the arc-related Buchans River Formation has established that the VMS deposits formed at ca. 465 Ma (Zagorevski et al. 2007*b*).

Geology of debris flow ore deposits at Buchans

Buchans ore deposits have been described by Thurlow (1977, 1981*b*); Thurlow and Swanson (1981); Stewart (1985), and Kirkham and Thurlow (1987). Approximately half of 17 Mt of high-grade ore at Buchans was mined from mechanically transported orebodies (see Fig. 1 for distribution). Transported orebodies associated with the Lucky Strike orebody (McLean, Rothermere, Two Level, and North) are separate, elongate sulfide breccia lenses associated with sulfide-bearing breccia–conglomerate and granite conglomerate, deposited in paleotopographic depressions and disposed in a linear arrangement extending northwest from Lucky Strike (Fig. 1; Binney 1987; Stewart 1987). Unlike the in situ orebodies, these transported deposits are not underlain by stockwork mineralization. These orebodies consist of varying proportions of angular to subrounded sulfide, barite, and lithic fragments, and they grade laterally into lower-grade breccia–conglomerate that contains sparse sulfide fragments. A complete continuum from high-grade, lithic-poor ore to barren, polylithic breccia–conglomerate is present. All lithic fragments, other than granitoid cobbles, are clearly, based on lithological features, of local origin, including "Intermediate Footwall" sequence (i.e., highly altered, silicified basaltic andesite and chloritized rhyodacite: van Hees et al. 2012), rhyolite, siltstone, and minor basaltic andesite. Enigmatic granitoid pebbles, cobbles, and boulders comprise less than 44% of clasts in the breccia horizons (Binney 1987). Thurlow and Swanson (1981) suggested two hypotheses for the origin of the granitoid clasts: (*i*) formation in "pebble dykes" like those associated with Japanese Kuroko deposits and (*ii*) derivation from an upfaulted, and subaerially exposed, plutonic island fringed by a cobble beach shoreline.

Summary of earlier work on granitoid cobbles

Stewart (1983, 1984, 1985, and 1987) carried out detailed geological, mineralogical, and geochemical studies of granitoid cobbles sampled in underground mining drifts of the McLean Extension ore horizon. All of these clast types are fine grained and likely represent either hypabyssal intrusions or interiors of slowly cooled felsic flows. Stewart (1984) classified the granitoid clasts into six types (see Table 1) and reduced clast types to "granitic" (Types 1 and 3), "aplitic" (Types 2, 4, and 5), and "other" (Type 6), based on average grain size and groundmass texture. The granitic group clasts are (*i*) typically the most highly rounded; (*ii*) commonly elongate or ovoid in shape; (*iii*) the largest in mean size of all clast types in the transported ore sequences; (*iv*) typically more pervasively hydrothermally altered prior to transport than aplitic group clasts; and (*v*) found intimately associated with the greatest concentration of sulfide mineralization. The aplitic group clasts are generally smaller and less altered, and they predominate in the less sulfidic debris flow units that overlie granitic cobble-rich, ore-grade debris flows. Type 6 lack quartz phenocrysts or granophyric patches, contain a greater proportion of "lath-like" plagioclase grains than other cobble types, and exhibit a lesser degree of pre-transport hydrothermal alteration. They are rare in MacLean Extension ore-zone debris flow units and are largely restricted to the siltstone breccia unit that underlies the ore zone. At the Old Buchans conglomerate orebody (Fig. 1) all lithic clast types, including granitoid cobbles, are well rounded. This greater abrasion suggested to Thurlow and Swanson (1981) that this orebody represented a reworked debris flow deposit. This interpretation is supported by our sampling in this study of four of the six granitoid cobble types (Types 1–3 and 6; Table 1) from the same stratigraphic horizon at this location.

Stewart (1984) noted that hydrothermal alteration of granitoid clasts was accompanied by introduction of barite and calcite, sericitization of plagioclase crystals, and chloritization of mafic phases (biotite and amphibole). This alteration is reflected by increased Ca, Ba, and Sr and loss on ignition (LOI). Granitic group samples exhibit the greatest degree of silicification and chloritization. In the aplitic group, calcite, barite, and quartz commonly occur as veins that predate deposition. Silicification of granitoid cobbles is reflected by anhydrous silica abundances in excess of 76 wt.% (up to 81%). Loss of potassium is most pronounced within the aplitic group and Little Sandy Lake granodiorite (LSLG). Overall, Stewart (1985) interpreted the alteration to be much more pronounced in the granitic group than the aplitic group. Other major (TiO_2, Al_2O_3, FeO^{total}, MgO, and P_2O_5) and minor (Ga, Nb, Y, and Zr) elements appear to show little evidence for mobility during alteration. In agreement with Thurlow (1981*a*, 1981*b*), Stewart (1985) concluded that the WBG and LSLG intrusions were high level and slightly more differentiated plutonic facies of the felsic

Fig. 1. (A) Regional tectonostratigraphy of Newfoundland and distribution of Darriwilian volcanic rocks in the Annieopsquotch accretionary tract. (B) Simplified geology of the Buchans mining camp. VMS occurrences (in situ (I) and transported (T)) are indicated for Buchans Group orebodies: 1, Halfway Mountain; 2, Skidder; 3, Clementine (T); 4, MacLean (T); 5, Rothermere (T), Level Two (T); 6, Lucky Strike (I); 7, Old Buchans (T); 8, Oriental (T and I); 9, Sandfill (T); 10, Engine House (I); 11, Middle Branch (T); 12,Woodmans Brook; 13, Little Sandy. Geochronology compiled from Coombs et al. (2012), Dunning et al. (1987), G. Dunning (personal communication, 2012), Zagorevski et al. (2006), and Zagorevski et al. (2007*b* and unpublished data). RIL, Red Indian Lake.

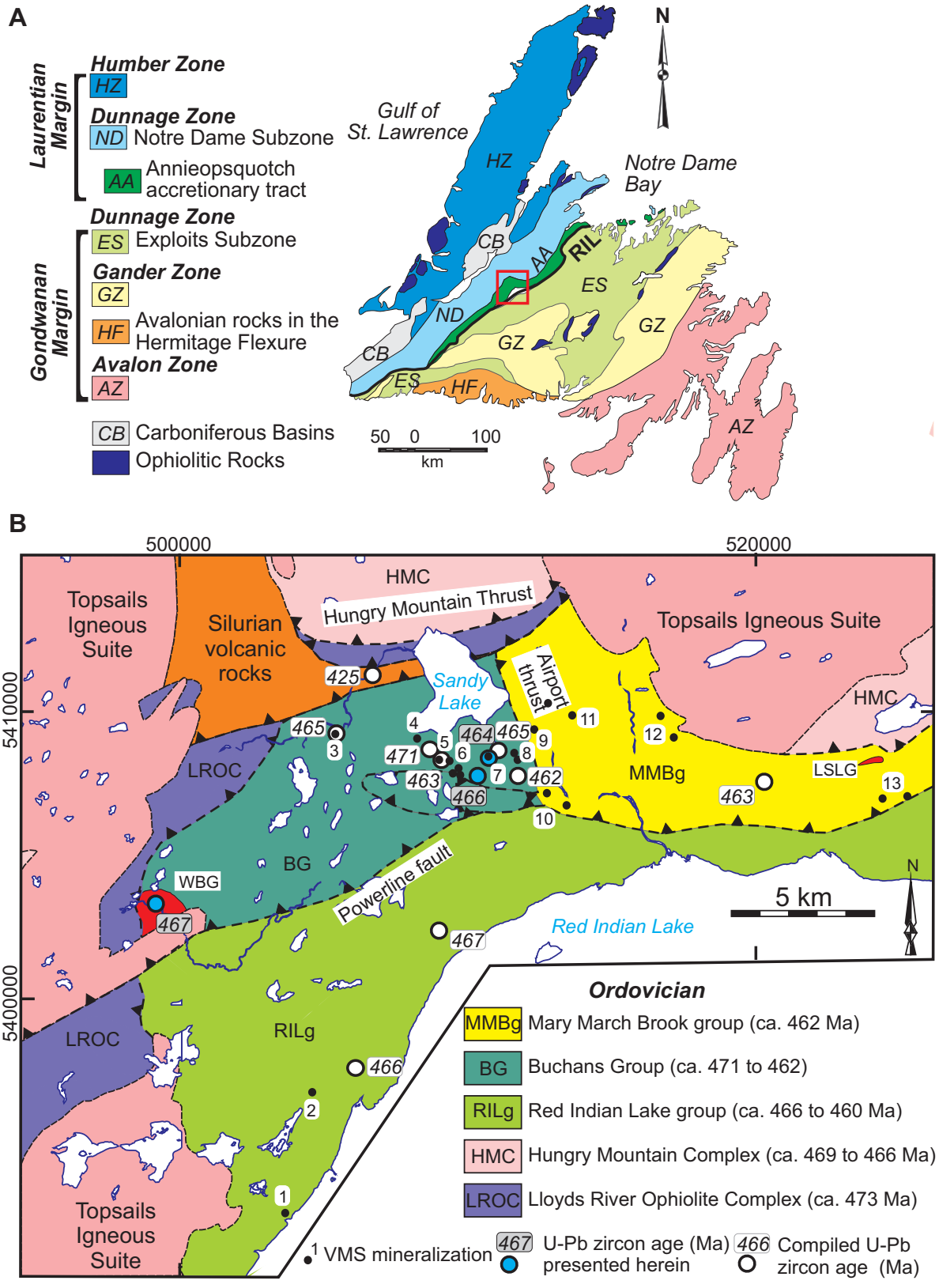

Table 1. Petrographic classification of granitoid clasts.

Clast type	Distinguishing features
1	Relatively coarse grained (0.2–3.0 mm), seriate texture, i.e., gradation in grain size of groundmass to qtz + feld phenocrysts (up to 5 mm)
2	Relatively intermediate grain size (0.1–2 mm) and equigranular, some qtz + feld phenocrysts (up to 2 mm)
3	Hiatal porphyritic, i.e., large difference in size between phenocrysts and groundmass; abundant qtz + feld phenocrysts (1–8 mm)
4	Equigranular, fine grain size (0.1–0.4 mm), only rare qtz + feld phenocrysts, minor granophyric areas
5	Very fine to fine grained (0.1–2 mm), abundant microgranophyre, equigranular, only rare qtz phenocrysts
6	Very fine grained (0.1–0.4 mm), "lath-like" texture of feld, abundant mafic minerals, no phenocrysts

Note: Based on table 1 of Stewart (1984). qtz, quartz; feld, feldspar.

volcanic activity that produced the Buchans rhyolites and granitoid clasts.

Stewart (1985, 1987) suggested that the granitoid clasts were altered, rounded, and transported to the surface in breccia pipes by explosive volatile activity that was probably due (at least in part) to the exsolution of an aqueous phase from the source magma chamber. Based on granitoid clast type stratigraphic distribution, Type 6 cobbles, which occur mainly with a breccia unit underlying the ore zone, were considered to be products of an early crystallized phase. This phase was followed by relatively slow magma solidification at moderate depths to yield the granitic group (Types 1 and 3; Table 1) clasts that are most abundant within the ore-grade horizon. Subsequently felsic magma was rapidly chilled, yielding intrusive rock from which the aplitic group (Types 2, 4, and 5) clasts were sourced and which predominate in overlying sulfide-poor debris units.

Geochronology

Three samples were collected for U–Pb zircon geochronology to provide constraints on the genesis of the granitoid cobbles hosted by the Buchans deposit. These samples include the WBG, which was interpreted to be co-magmatic with the cobbles (Thurlow 1981*b*; Stewart 1983, 1987), a granitoid clast from the Buchans River Formation conglomerate unit at the Buchans mine site, and a sample of Buchans River Formation conglomerate from drill core. These samples were analyzed at the Geological Survey of Canada (GSC) using either U–Pb isotope dilution – thermal ionization mass spectrometry (ID–TIMS) or in situ sensitive high-resolution ion microprobe (SHRIMP) techniques. Numbers given later in the text after sample type correspond to field number and U–Pb lab number, respectively. See Appendix A for analytical methods.

Sample descriptions and age interpretations

Wiley's Brook granodiorite (RAX06A186; z9103)

The Wiley's Brook granodiorite (WBG) occupies an area of approximately 1.5 km^2 in the westernmost part of the Buchans Group (Fig. 1) and was considered the subvolcanic equivalent to the Buchans Group felsic volcanic rocks (i.e., "Feeder" granodiorite of Thurlow and Swanson (1981)). Granitoid clasts within the Buchans orebodies were correlated to the WBG by Stewart (1983, 1987), with their presence attributed to in situ brecciation and transport to the surface by phreatic (caused by magmatic heat) steam eruption (Sillitoe 1985). The sample was collected to test the proposed relationship to Buchans Group felsic volcanic rocks. The sample consisted of massive, beige to hematized, medium-grained tonalite to granodiorite, characterized by large quartz glomerocrysts up to 1 cm in diameter and minor chloritized biotite.

The granodiorite sample yielded abundant high-quality zircon crystals ranging in morphology from stubby prismatic to prismatic grains. Five abraded multigrain zircon fractions were analyzed using ID–TIMS techniques (Table 2). All of the analyses overlap each other and concordia, with no evidence of inheritance or lead loss (Fig. 2*a*). A concordia age is calculated to be 466.7 ± 0.5 Ma (mean square weighted deviation (MSWD) of concordance and equivalence = 0.84, probability = 0.58, n = 5), which is interpreted to be the crystallization age of the WBG.

Buchans conglomerate clast (KQ-84-32B; z10720)

An ovoid 10 cm granitoid clast was extracted from a sample of Buchans River Formation polylithic conglomerate collected in 1984 by R. Kirkham from a surface stockpile at the Buchans mine site. In the classification scheme of Stewart (1984) (Table 1), this is a Type 3 granitoid cobble.

The clast yielded a small number of euhedral zircons, ranging in morphology from equant crystals to stubby prismatic grains. The zircon grains are quite small (<75 μm; majority 30–60 μm in size). Some of the grains are clear, but the majority contain numerous fractures and inclusions. Because the zircon grains are quite small and of poor to fair quality, they were analyzed using SHRIMP techniques. Back-scattered electron (BSE) and cathodoluminescence (CL) scanning electron microscopy (SEM) images reveal well-defined growth zoning in many grains. The majority of the SHRIMP analyses define a single age population (Fig. 2*b*), and a weighted average of the $^{206}Pb/^{238}U$ ages is calculated as 463.7 ± 1.8 Ma (MSWD = 1.2, probability = 0.19, n = 37). One analyzed zircon grain has an age of ca. 497 Ma (analysis 47.1, Table 3) and is interpreted to be inherited in origin. Taking into account the error associated with the zircon standards analyzed on the SHRIMP grain mount, the crystallization age of the granitoid clast is interpreted to be 464 ± 4 Ma.

Buchans River Formation conglomerate (RAX06012; z8974)

A sample of Buchans River Formation granitoid-bearing conglomerate was obtained from drill core (DDH HG266-3 164–165 m). It consisted mainly of the gritty arenaceous matrix but did include some small granitoid cobbles.

The conglomerate yielded abundant zircons ranging in size from 50 to 200 μm, including equant, multifaceted crystals, stubby prismatic to prismatic grains, and elongate crystals. BSE-SEM imaging revealed faint to well-defined growth zoning in many of the grains, as well as grains with core–rim relationships. SHRIMP analyses ranging in age from ca. 543–1500 Ma (Fig. 2*d*, Table 3) are from inherited cores within detrital zircon grains (Fig. 2*e*). A $^{206}Pb/^{238}U$ weighted average age of the dominant youngest age population is calculated to be 465.9 ± 1.9 (MSWD = 0.71; probability = 0.94; n = 57). These youngest analyses are from entire magmatic grains with well-defined growth zoning, as well as from rims of grains with inherited cores (Fig. 2*e*, grain 14). Taking into account the error associated with the zircon standards analyzed on the SHRIMP mount, the maximum age of deposition of the conglomerate–sandstone sequence and the age of the youngest volcanoplutonic source is interpreted to be 466 ± 4 Ma.

Discussion of geochronology results

The new ages presented herein for the WBG (466.7 ± 0.5 Ma), the Buchans River Formation granitoid cobble (464 ± 4 Ma), and the maximum age of detritus from the Buchans River Formation conglomerate–sandstone sequence (466 ± 4 Ma) are indistinguishable from dates obtained from felsic volcanic units that host the Buchans VMS deposits (Zagorevski et al. 2007*b*). The U–Pb zircon ages obtained from the Buchans Group felsic volcanic and plutonic rocks are within analytical error and are consistent with the in-

Table 2. U–Pb ID–TIMS analytical data for Wiley's Brook granodiorite: RAX06A186 (z9103).

Fraction[c]	Description[d]	Wt. (μg)	U (ppm)	Pb[e] (ppm)	$^{206}Pb/^{204}Pb$	Pb[g] (pg)	Isotopic ratios[a]								Ages (Ma)[b]						Disc. (%)
					[f]		$^{208}Pb/^{206}Pb$	$^{207}Pb/^{235}U$	±1 SE (abs)	$^{206}Pb/^{238}U$	±1 SE (abs)	Corr. coeff.[h]	$^{207}Pb/^{206}Pb$	±1 SE (abs)	$^{206}Pb/^{238}U$	±2 SE	$^{207}Pb/^{235}U$	±2 SE	$^{207}Pb/^{206}Pb$	±2 SE	
A1 (Z;6)	Co, Clr, Eu, St, fln	24	75	6	886	10	0.17	0.58184	0.00161	0.07495	0.00009	0.606	0.05631	0.00013	465.9	1.0	465.6	2.1	464.5	10.0	–0.3
B1 (Z;19)	Co, Clr, Eu, St, rln	13	141	11	1890	4	0.18	0.58486	0.00116	0.07513	0.00007	0.676	0.05646	0.00009	467.0	0.8	467.6	1.5	470.6	6.7	0.8
C1 (Z;6)	Co, Clr, Eu, Pr, fln	24	110	9	5992	2	0.18	0.58306	0.00090	0.07493	0.00012	0.736	0.05643	0.00006	465.8	1.4	466.4	1.2	469.5	4.9	0.8
C2 (Z;8)	Co, Clr, Eu, Pr, fln	22	112	9	4864	2	0.18	0.58446	0.00083	0.07506	0.00009	0.793	0.05647	0.00005	466.6	1.1	467.3	1.1	470.9	3.9	1.0
D1 (Z;18)	Co, Clr, Eu, Pr, rln	12	201	16	1438	8	0.18	0.58368	0.00119	0.07511	0.00007	0.664	0.05636	0.00009	466.9	0.9	466.8	1.5	466.7	6.9	0.0

Note: Universal Transverse Mercator (UTM) North American Datum 1983 (NAD83) zone 21, 499463E, 5402844 N. Disc., discordance; SE, standard error; Wt., weight.

[a]Corrected for blank Pb and U and common Pb, errors quoted are 1σ absolute (abs); procedural blank values for this study ranged from <0.1– 0.1 pg for U and 0.5–2 pg for Pb; Pb blank isotopic composition is based on the analysis of procedural blanks; corrections for common Pb were made using Stacey–Kramers compositions.

[b]Corrected for blank and common Pb, errors quoted are 2σ in Ma.

[c]Z, zircon. Number in bracket refers to the number of grains in the analysis.

[d]Fraction descriptions: Co, colourless; Clr, clear; Eu, euhedral; Pr, prismatic; St, stubby prism; rln, rare inclusions; fln, few inclusions.

[e]Radiogenic Pb.

[f]Measured ratio, corrected for spike and fractionation.

[g]Total common Pb in analysis corrected for fractionation and spike.

[h]Correlation coefficient.

terpretation that the felsic extrusive and plutonic rocks are consanguineous (Thurlow 1981*b*; Stewart 1983, 1987).

Geochemistry

Introduction

New geochemical and Nd isotopic data presented herein were obtained from 17 granitoid cobble samples collected from surface exposures of conglomerate at the Old Buchans deposit. Classification of these samples based on the granitoid grain size and textural criteria of Stewart (1985) (Table 1) yielded five samples of Type 1, six samples of Type 2, three samples of Type 3, and three samples of Type 6 cobbles. Samples of granodiorite exposed in WBG (two samples) and adjacent to Little Sandy Lake (LSLG, one sample) were also collected. All samples were analyzed for major elements and an extensive range of trace elements (see Zagorevski and Rogers (2011) and Table 4). Unpublished geochemical analyses of granitoid cobbles, WBG, and LSLG were also utilized in this study (Stewart 1985). Comparisons are made with felsic volcanic units contained within the Buchans Group and adjacent structural panels. Stewart (1985, 1987) documented that hydrothermal alteration of granitoid cobbles was accompanied by mobility of Ca, Ba, Sr, K, and Si (see earlier in the text). These alteration effects need to be kept in mind when making inferences based on whole-rock geochemistry concerning granitic intrusions from which the cobbles were derived.

Major and trace elements

Based on the International Union of Geological Sciences normative Q′ (100[Q/(Q + Or + Ab + An)]) – ANOR (100[An/(Or + An)]) granitoid rock classification diagram of Streckeisen and Le Maitre (1979) (Fig. 3), samples consist mainly of tonalite and granodiorite but with minor monzogranite and calcic tonalite. Silicification of both granitic group (Types 1 and 3) and aplitic group (Types 2, 4, and 5) cobbles is clearly indicated by Q′ values ranging mainly between 45 and 55, whereas Q′ values of less altered Type 6 cobbles, WBG, and LSLG samples range from 29 to 47. Addition of hydrothermal calcite within veins likely caused a shift of some aplitic group samples from the tonalite to calcic tonalite field (Fig. 3). Samples plot adjacent to (least-altered WBG and Type 6 cobble samples) or well above (LSLG and other cobble samples) trends defined by calcic primitive arc plutonic suites such as the Coast Range batholith of California and an oceanic arc suite in New Britain, Papua New Guinea (labelled C and NB in Fig. 3).

In the three-tiered major element – based classification scheme for granitoid rocks of Frost et al. (2001): (*i*) All samples are magnesian (oxidized) (Fig. 4*a*). FeO and MgO are interpreted as immobile during alteration at Buchans (Stewart 1985, 1987). (*ii*) Almost all samples are calcic with relatively unaltered Type 6 cobble, WBG, and LSLG samples plotting mainly in the calcic A field (Fig. 4*b*). Lower modified-alkali lime index (MALI) values of other cobble types likely reflects hydrothermal introduction of calcite. (*iii*) Many granitoid samples exhibit aluminum saturation index (ASI) (Al/(Ca – 1.67P + Na + K)) values in excess of 1.1 (not shown), an S-type granite characteristic (White and Chappell 1988). However, some Type 6 cobbles and WBG samples contain altered or fresh hornblende and clinopyroxene, indicative of a primary metaluminous character. Therefore, high ASI values are attributed to alkali element mobility, not crystallization from peraluminous (possibly S-type) felsic magmas.

Because of silicification, Harker diagrams are not a reliable tool for evaluating chemical variation and co-magmatism within the felsic igneous rocks of the Buchans Camp. Instead of SiO_2, FeO^{total} was employed for Harker-like plots (Fig. 5; see White and Chappell 1988). In plots of FeO^{total} versus CaO, Na_2O, LOI, and Sr, most granitoid cobble types exhibit a similar high degree of scatter at low FeO^{total} levels owing to hydrothermal addition of calcite and barite and sericitization of feldspar. In contrast, the less altered

Fig. 2. (*a*) Concordia diagram of U–Pb ID–TIMS zircon analyses from the WBG. (*b*) Concordia diagram of U–Pb SHRIMP zircon analyses from a granitoid clast in the Buchans River Formation (Fm) conglomerate. (*c*) Dated Type 3 granitoid cobble KQ-84-32B. (*d*) Concordia diagram of U–Pb SHRIMP detrital zircon analyses from a sample of Buchans River Formation conglomerate. (*e*) BSE-SEM images of detrital zircons from the Buchans River Formation conglomerate showing location and ages of SHRIMP analyses.

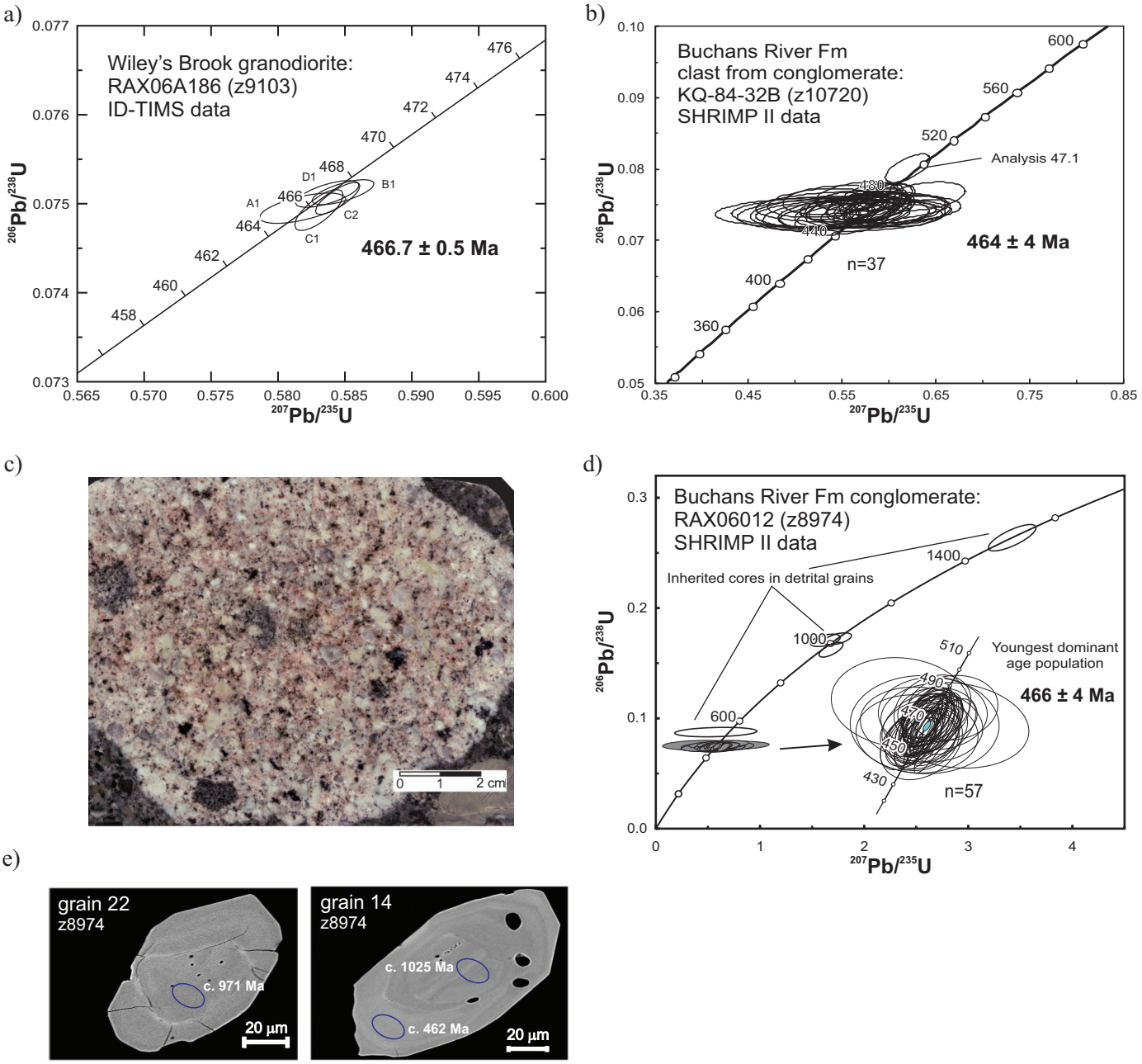

Type 6 cobbles and relatively fresh WBG and LSLG samples exhibit apparently collinear positive correlations with FeO^{total}. For elements that were found by Stewart (1985, 1987) to be relatively unaffected by alteration, such as TiO_2, Al_2O_3, MgO, and V, all samples exhibit fairly collinear positive trends. For Y and Zr, elements that would be expected to be relatively immobile during alteration, the cobble samples exhibit a large degree of variation, possibly because of the small size of analyzed cobbles and control by accessory minerals such as zircon, allanite, and monazite. Thorium, which is often used as a fractionation index in volcanic rock suites, exhibits a negative trend with FeO^{total}. A negative correlation can be expected if most of the cobbles crystallized from a more fractionated magma than the less evolved source magma for Type 6 cobbles, WBG, and LSLG. In general, collinear behaviour of both cobble and pluton samples in these plots for elements least affected by alteration is generally permissive of a co-magmatic origin. However, higher TiO_2 and MgO contents within most Type 2 cobbles may reflect derivation from a somewhat different magma source.

On primitive mantle-normalized extended-element diagrams (Fig. 6), all samples exhibit very similar patterns, with pronounced negative Nb and Ti anomalies and variable negative Sr and P anomalies. Positive Th anomalies observed in Type 1–3 cobbles and to a lesser degree in felsic volcanic rocks likely reflect alteration-related depletion in Rb and K and not a real enrichment in Th.

To better examine elemental differences between these samples, they have been normalized to the average WBG composition

Table 3. U–Pb SHRIMP analytical data.

Spot name	U (ppm)	Th (ppm)	Th/U	$^{206}Pb^*$ (ppm)	$^{204}Pb/^{206}Pb$	% ±	$f(206)^{204}$ (%)	$^{208*}Pb/^{206*}Pb$	±$^{208}Pb/^{206}Pb$	$^{207*}Pb/^{235}U$	±$^{207}Pb/^{235}U$	$^{206*}Pb/^{238}U$	±$^{206}Pb/^{238}U$	Corr. coeff.	$^{207*}Pb/^{206*}Pb$	±$^{207}Pb/^{206}Pb$	Apparent ages (Ma) $^{206}Pb/^{238}U$	±$^{206}Pb/^{238}U$	$^{207}Pb/^{206}Pb$	±$^{207}Pb/^{206}Pb$	Disc. (%)	Yb (ppm)	Hf (ppm)
Buchans River Formation clast from conglomerate: KQ-84-32B (z10720)																							
10720-1.1	390	250	0.64	25	4.1×10^{-5}	98	0.071	0.0237	0.0004	0.5821	0.0121	0.0744	0.0008	0.523	0.0568	0.0010	462.4	4.9	471	15	4.4	437	9869
10720-9.1	322	227	0.71	21	-1.7×10^{-4}	54	−0.292	0.0249	0.0007	0.6364	0.0181	0.0762	0.0008	0.379	0.0606	0.0016	473.4	4.9	510	18	25.1	575	9726
10720-10.1	310	162	0.52	20	-6.9×10^{-5}	61	−0.120	0.0232	0.0004	0.5954	0.0130	0.0760	0.0008	0.477	0.0568	0.0011	472.3	4.7	470	18	2.5	466	9679
10720-16.2	213	102	0.48	13	1.1×10^{-4}	39	0.197	0.0267	0.0006	0.6291	0.0148	0.0738	0.0008	0.448	0.0618	0.0013	459.3	4.7	519	22	32.3	297	9994
10720-11.1	115	42	0.36	7	1.5×10^{-4}	80	0.253	0.0248	0.0011	0.5232	0.0233	0.0734	0.0008	0.249	0.0517	0.0022	456.3	4.9	474	36	−69.3	256	9537
10720-13.1	191	91	0.48	12	2.0×10^{-4}	164	0.350	0.0250	0.0024	0.5407	0.0512	0.0740	0.0009	0.127	0.0530	0.0050	460.1	5.3	477	43	−41.1	395	9383
10720-21.1	256	180	0.70	16	-3.5×10^{-5}	74	−0.061	0.0234	0.0004	0.5925	0.0127	0.0740	0.0008	0.487	0.0581	0.0011	459.9	4.6	470	17	14.3	478	9950
10720-23.1	239	99	0.41	15	3.9×10^{-4}	29	0.680	0.0236	0.0009	0.5342	0.0212	0.0736	0.0008	0.270	0.0526	0.0020	457.8	4.7	421	32	−47.7	426	9843
10720-27.1	159	85	0.53	10	2.7×10^{-4}	39	0.467	0.0267	0.0010	0.5409	0.0219	0.0757	0.0008	0.269	0.0518	0.0020	470.6	4.9	505	27	−72.8	356	9813
10720-28.1	319	296	0.93	20	1.0×10^{-4}	44	0.182	0.0260	0.0005	0.5904	0.0131	0.0747	0.0008	0.468	0.0574	0.0011	464.1	4.7	512	18	8.5	290	9819
10720-29.1	231	97	0.42	15	3.1×10^{-4}	31	0.542	0.0250	0.0008	0.5633	0.0197	0.0743	0.0008	0.306	0.0550	0.0018	461.9	4.8	459	26	−12.5	442	9514
10720-31.1	171	77	0.45	11	4.3×10^{-4}	33	0.751	0.0240	0.0012	0.5179	0.0264	0.0739	0.0008	0.218	0.0509	0.0025	459.3	4.9	429	30	−99.5	244	10673
10720-32.1	232	110	0.48	15	4.1×10^{-4}	30	0.710	0.0239	0.0010	0.5291	0.0236	0.0753	0.0008	0.243	0.0510	0.0022	468.0	4.9	430	26	−99.5	400	10289
10720-34.1	133	56	0.42	9	8.0×10^{-4}	31	1.380	0.0230	0.0017	0.5611	0.0418	0.0748	0.0009	0.159	0.0544	0.0040	464.8	5.3	357	41	−20.3	270	9206
10720-36.1	294	164	0.56	19	1.6×10^{-4}	36	0.285	0.0243	0.0007	0.6137	0.0188	0.0744	0.0008	0.345	0.0598	0.0017	462.6	4.7	470	20	23.4	506	9591
10720-39.1	290	126	0.43	19	-1.3×10^{-6}	7164	−0.002	0.0225	0.0007	0.5811	0.0191	0.0749	0.0008	0.335	0.0563	0.0017	465.4	4.9	450	24	−0.3	482	10135
10720-41.1	351	232	0.66	23	-8.4×10^{-5}	70	−0.146	0.0247	0.0005	0.5885	0.0145	0.0748	0.0008	0.426	0.0571	0.0013	465.0	4.7	499	17	6.1	368	10490
10720-44.1	304	177	0.58	20	-2.7×10^{-5}	38	−0.046	0.0227	0.0004	0.5894	0.0123	0.0754	0.0008	0.501	0.0567	0.0010	468.5	4.7	456	18	2.5	305	10112
10720-50.1	219	137	0.62	14	1.8×10^{-4}	43	0.306	0.0265	0.0008	0.5657	0.0178	0.0763	0.0008	0.340	0.0538	0.0016	473.8	4.9	512	22	−31.9	358	9938
10720-51.1	255	147	0.58	16	5.5×10^{-5}	242	0.095	0.0243	0.0009	0.5854	0.0234	0.0737	0.0008	0.270	0.0576	0.0022	458.3	4.8	481	23	11.5	485	9504
10720-54.1	158	58	0.37	10	1.2×10^{-4}	53	0.203	0.0258	0.0008	0.5557	0.0181	0.0740	0.0008	0.334	0.0545	0.0017	460.0	4.8	498	33	−18.2	296	10350
10720-53.1	258	106	0.41	16	1.8×10^{-4}	121	0.308	0.0237	0.0014	0.5908	0.0349	0.0744	0.0008	0.189	0.0576	0.0033	462.9	5.0	450	36	10.1	455	10119
10720-55.1	511	236	0.46	33	2.3×10^{-5}	97	0.039	0.0243	0.0004	0.5886	0.0106	0.0761	0.0008	0.579	0.0561	0.0008	472.8	4.7	482	16	−3.8	595	10255
10720-59.1	85	32	0.37	5	5.0×10^{-4}	42	0.860	0.0262	0.0018	0.5306	0.0374	0.0737	0.0009	0.171	0.0522	0.0036	458.3	5.3	453	48	−57.1	176	10427
10720-60.1	196	104	0.53	12	3.3×10^{-4}	38	0.566	0.0236	0.0010	0.5575	0.0234	0.0738	0.0008	0.259	0.0548	0.0022	458.8	4.8	439	25	−13.8	389	9413
10720-61.1	373	222	0.60	24	8.3×10^{-5}	30	0.143	0.0229	0.0004	0.5787	0.0113	0.0743	0.0008	0.543	0.0565	0.0009	462.2	4.7	451	21	1.9	503	10194
10720-64.1	242	104	0.43	15	1.4×10^{-4}	20	0.248	0.0245	0.0005	0.5735	0.0131	0.0738	0.0008	0.458	0.0563	0.0011	459.2	4.7	472	22	1.4	434	9588
10720-71.1	254	123	0.49	16	1.3×10^{-4}	18	0.223	0.0253	0.0005	0.5416	0.0122	0.0749	0.0008	0.464	0.0525	0.0011	465.3	4.7	490	20	−53.8	427	9860
10720-75.1	131	51	0.39	8	1.4×10^{-4}	205	0.235	0.0235	0.0019	0.5416	0.0443	0.0741	0.0009	0.145	0.0530	0.0043	460.7	5.3	450	48	−41.1	280	10212
10720-77.1	326	160	0.49	21	1.8×10^{-5}	290	0.031	0.0263	0.0006	0.5805	0.0136	0.0756	0.0008	0.445	0.0557	0.0012	469.7	4.7	523	20	−6.8	491	10143
10720-76.1	370	193	0.52	24	3.5×10^{-5}	67	0.061	0.0247	0.0004	0.5694	0.0111	0.0749	0.0008	0.531	0.0552	0.0009	465.3	4.6	489	17	−11.5	559	9981
10720-78.1	173	86	0.49	11	1.1×10^{-4}	95	0.186	0.0218	0.0008	0.5509	0.0205	0.0730	0.0009	0.330	0.0547	0.0019	454.1	5.4	424	25	−13.6	304	10028
10720-79.1	226	121	0.54	14	1.5×10^{-4}	149	0.257	0.0243	0.0015	0.5702	0.0351	0.0734	0.0008	0.182	0.0564	0.0034	456.4	4.9	471	30	2.3	324	10185
10720-83.1	303	170	0.56	19	1.3×10^{-4}	212	0.218	0.0239	0.0017	0.5593	0.0411	0.0738	0.0008	0.155	0.0550	0.0040	458.8	5.0	465	30	−11.8	363	10179
10720-84.1	312	166	0.53	20	-6.3×10^{-5}	95	−0.108	0.0242	0.0005	0.5833	0.0143	0.0749	0.0008	0.425	0.0565	0.0013	465.9	4.7	489	19	1.0	424	9972
10720-85.1	285	142	0.50	18	9.9×10^{-5}	43	0.172	0.0248	0.0005	0.5660	0.0132	0.0746	0.0008	0.455	0.0550	0.0011	464.1	4.7	485	20	−13.1	478	9951
10720-89.1	237	145	0.61	16	8.8×10^{-5}	68	0.152	0.0264	0.0006	0.5864	0.0157	0.0761	0.0008	0.394	0.0559	0.0014	473.0	4.8	519	20	−6.1	417	9911
10720-47.1	861	711	0.83	59	-3.4×10^{-6}	739	−0.006	0.0258	0.0003	0.6202	0.0097	0.0802	0.0008	0.650	0.0561	0.0007	497.0	4.9	516	11	−9.1	853	9757

Grain mount IP655; spot size 17 μm × 23 μm; no. of scans, 5; error in $^{206}Pb/^{238}U$ calibration, 1.0% (included). Uncertainties are calculated by using SQUID 2.23.08.10.21, revised 21 October 2008.

Spot name	U (ppm)	Th (ppm)	Th/U	Pb* (ppm)	^{204}Pb (ppb)	$^{204}Pb/^{206}Pb$	±$^{204}Pb/^{206}Pb$	$f(206)^{204}$ (%)	$^{208*}Pb/^{206*}Pb$	±$^{208}Pb/^{206}Pb$	$^{207*}Pb/^{235}U$	±$^{207}Pb/^{235}U$	$^{206*}Pb/^{238}U$	±$^{206}Pb/^{238}U$	Corr. coeff.	$^{207*}Pb/^{206*}Pb$	±$^{207}Pb/^{206}Pb$	$^{206}Pb/^{238}U$	±$^{206}Pb/^{238}U$	$^{207}Pb/^{206}Pb$	±$^{207}Pb/^{206}Pb$	Disc. (%)
Buchans River Formation conglomerate: RAX06012 (z8974); DDH HG266-3 from 164 to 165 m																						
8974-2.1	175	131	0.771	15	0	0.000010	0.000010	0.0002	0.2433	0.0052	0.615	0.080	0.0762	0.0011	0.230	0.0585	0.0075	473.5	6.4	549	306	13.7
8974-4.1	107	85	0.821	9	1	0.000209	0.000300	0.0036	0.2637	0.0136	0.592	0.064	0.0736	0.0011	0.265	0.0584	0.0061	457.5	6.8	545	246	16.0
8974-5.1	130	75	0.597	10	2	0.000259	0.000233	0.0045	0.1915	0.0104	0.569	0.048	0.0745	0.0011	0.296	0.0555	0.0045	463.0	6.7	431	194	−7.5
8974-6.1	87	58	0.688	7	4	0.000704	0.000263	0.0122	0.2219	0.0211	0.517	0.046	0.0732	0.0012	0.307	0.0512	0.0044	455.4	7.4	251	211	−81.7
8974-8.1	141	118	0.866	12	3	0.000370	0.000163	0.0064	0.2645	0.0089	0.570	0.038	0.0738	0.0011	0.343	0.0560	0.0035	459.0	6.7	452	147	−1.5
8974-9.1	356	305	0.885	31	7	0.000281	0.000088	0.0049	0.2797	0.0056	0.561	0.018	0.0757	0.0009	0.484	0.0537	0.0016	470.3	5.6	359	67	−31.0
8974-10.1	138	77	0.577	11	1	0.000144	0.000227	0.0025	0.1766	0.0115	0.633	0.042	0.0751	0.0013	0.380	0.0612	0.0038	466.6	7.8	647	138	27.8

Table 3 (*concluded*).

Spot name	U (ppm)	Th (ppm)	Th/U	Pb* (ppm)	^{204}Pb (ppb)	^{204}Pb/^{206}Pb	±^{204}Pb/^{206}Pb	$f(206)^{204}$ (%)	^{208*}Pb/^{206*}Pb	±^{208}Pb/^{206}Pb	^{207*}Pb/^{235}U	±^{207}Pb/^{235}U	^{206*}Pb/^{238}U	±^{206}Pb/^{238}U	Corr. coeff.	^{207*}Pb/^{206*}Pb	±^{207}Pb/^{206}Pb	^{206}Pb/^{238}U	±^{206}Pb/^{238}U	^{207}Pb/^{206}Pb	±^{207}Pb/^{206}Pb	Disc. (%)
8974-11.1	93	62	0.696	8	1	0.000117	0.000214	0.0020	0.2384	0.0188	0.630	0.040	0.0751	0.0010	0.336	0.0609	0.0036	466.6	6.1	634	134	26.4
8974-13.1	74	72	1.000	7	2	0.000516	0.000249	0.0089	0.3189	0.0229	0.635	0.047	0.0742	0.0012	0.335	0.0621	0.0043	461.2	7.1	679	157	32.1
8974-14.1	326	234	0.742	27	2	0.000111	0.000082	0.0019	0.2358	0.0092	0.589	0.018	0.0743	0.0010	0.556	0.0575	0.0015	462.2	6.2	510	58	9.3
8974-15.1	71	36	0.521	5	3	0.000564	0.000420	0.0098	0.1592	0.0170	0.588	0.072	0.0736	0.0012	0.256	0.0580	0.0069	457.5	7.2	529	284	13.6
8974-16.1	164	97	0.611	13	4	0.000412	0.000191	0.0071	0.1839	0.0122	0.559	0.034	0.0732	0.0010	0.344	0.0554	0.0032	455.2	6.0	429	133	−6.0
8974-18.1	168	89	0.550	13	4	0.000326	0.000273	0.0057	0.1704	0.0126	0.580	0.047	0.0757	0.0010	0.280	0.0556	0.0044	470.6	5.9	435	186	−8.1
8974-19.1	199	139	0.722	16	4	0.000279	0.000127	0.0048	0.2256	0.0069	0.566	0.026	0.0742	0.0010	0.394	0.0554	0.0024	461.1	5.7	428	99	−7.8
8974-20.1	244	164	0.695	20	0	0.000010	0.000010	0.0002	0.2215	0.0068	0.572	0.015	0.0741	0.0012	0.704	0.0560	0.0011	460.8	7.4	453	44	−1.6
8974-21.1	232	160	0.713	19	3	0.000199	0.000154	0.0035	0.2183	0.0074	0.561	0.029	0.0752	0.0010	0.385	0.0541	0.0026	467.5	6.3	373	112	−25.2
8974-23.1	228	194	0.876	20	5	0.000326	0.000192	0.0057	0.2653	0.0128	0.552	0.035	0.0756	0.0012	0.373	0.0530	0.0032	469.7	7.4	327	142	−43.8
8974-24.1	262	224	0.884	23	3	0.000156	0.000078	0.0027	0.2697	0.0056	0.594	0.021	0.0760	0.0010	0.479	0.0567	0.0018	472.3	6.0	479	71	1.4
8974-25.1	50	45	0.930	5	2	0.000629	0.000409	0.0109	0.3163	0.0267	0.580	0.073	0.0766	0.0013	0.261	0.0549	0.0067	475.9	8.0	408	300	−16.5
8974-26.1	30	23	0.796	2	5	0.002319	0.000823	0.0402	0.2070	0.0492	0.416	0.142	0.0762	0.0017	0.189	0.0396	0.0134	473.1	10.2	0	0	0.0
8974-28.1	77	54	0.729	6	2	0.000475	0.000653	0.0082	0.2228	0.0316	0.591	0.111	0.0762	0.0014	0.221	0.0563	0.0104	473.2	8.4	463	460	−2.3
8974-29.1	125	101	0.836	11	2	0.000274	0.000301	0.0048	0.2619	0.0503	0.583	0.054	0.0750	0.0015	0.332	0.0563	0.0049	466.3	8.8	466	207	−0.2
8974-30.1	286	210	0.759	24	7	0.000360	0.000172	0.0062	0.2298	0.0080	0.571	0.033	0.0761	0.0012	0.392	0.0544	0.0030	472.6	7.4	389	126	−21.5
8974-32.1	122	71	0.600	10	4	0.000463	0.000298	0.0080	0.1806	0.0149	0.610	0.053	0.0753	0.0013	0.310	0.0588	0.0049	468.3	7.5	558	193	16.2
8974-37.1	101	67	0.681	8	0	0.000010	0.000010	0.0002	0.2307	0.0075	0.656	0.024	0.0744	0.0015	0.655	0.0640	0.0018	462.3	9.2	741	60	37.6
8974-38.1	175	64	0.380	13	6	0.000499	0.000272	0.0086	0.1128	0.0107	0.565	0.048	0.07611	0.00104	0.282	0.0539	0.0044	472.9	6.2	365	197	−29.5
8974-39.1	41	38	0.956	4	5	0.001956	0.000670	0.0339	0.2899	0.0327	0.557	0.126	0.0749	0.00142	0.207	0.0540	0.0120	465.6	8.5	369	436	−26.2
8974-41.1	122	75	0.640	10	1	0.000175	0.000116	0.0030	0.1970	0.0068	0.589	0.029	0.0744	0.001	0.387	0.0574	0.0027	462.6	6.0	508	105	9.0
8974-42.1	438	392	0.926	38	2	0.000071	0.000037	0.0012	0.2905	0.0042	0.588	0.014	0.07501	0.00101	0.655	0.0569	0.0010	466.3	6.1	487	41	4.2
8974-43.1	23	17	0.753	2	2	0.001536	0.000860	0.0266	0.2528	0.0455	0.572	0.151	0.07498	0.0019	0.219	0.0554	0.0144	466.1	11.4	427	493	−9.2
8974-44.1	68	47	0.718	6	3	0.000787	0.000481	0.0136	0.2084	0.0199	0.580	0.082	0.07465	0.00139	0.253	0.0563	0.0078	464.1	8.4	466	341	0.4
8974-45.1	135	109	0.832	12	2	0.000233	0.000266	0.0040	0.2701	0.0188	0.583	0.049	0.07541	0.00099	0.277	0.0561	0.0046	468.7	5.9	456	192	−2.9
8974-46.1	155	125	0.833	13	3	0.000305	0.000250	0.0053	0.2542	0.0109	0.614	0.052	0.07532	0.0012	0.309	0.0591	0.0048	468.1	7.2	571	186	18.0
8974-47.1	104	68	0.671	9	4	0.000661	0.000269	0.0115	0.2259	0.0128	0.582	0.049	0.07495	0.00123	0.316	0.0564	0.0045	465.9	7.4	466	188	0.1
8974-48.1	115	75	0.678	10	5	0.000648	0.000230	0.0112	0.2172	0.0116	0.575	0.042	0.07561	0.00115	0.327	0.0551	0.0038	469.9	6.9	417	163	−12.8
8974-49.1	263	179	0.704	21	6	0.000336	0.000131	0.0058	0.2150	0.0063	0.563	0.025	0.07443	0.00108	0.439	0.0549	0.0022	462.8	6.5	408	93	−13.5
8974-50.1	140	154	1.140	13	5	0.000508	0.000200	0.0088	0.3423	0.0105	0.572	0.037	0.07475	0.00115	0.357	0.0555	0.0034	464.7	6.9	432	141	−7.5
8974-51.1	153	146	0.981	14	4	0.000381	0.000265	0.0066	0.3054	0.0119	0.583	0.047	0.07576	0.00119	0.316	0.0558	0.0043	470.8	7.1	446	180	−5.7
8974-52.1	92	60	0.671	8	0	0.000025	0.000258	0.0004	0.2374	0.0137	0.692	0.047	0.07552	0.00116	0.344	0.0665	0.0043	469.3	6.9	821	140	42.8
8974-53.1	28	16	0.579	2	3	0.001870	0.000740	0.0324	0.1670	0.0301	0.552	0.124	0.07398	0.0015	0.213	0.0542	0.0120	460.1	9.0	378	434	−21.8
8974-54.1	421	309	0.758	35	6	0.000230	0.000090	0.0040	0.2351	0.0088	0.583	0.040	0.07559	0.00096	0.306	0.0560	0.0037	469.7	5.7	451	152	−4.0
8974-55.1	322	211	0.678	26	8	0.000414	0.000145	0.0072	0.2173	0.0069	0.575	0.039	0.07317	0.00109	0.340	0.0570	0.0037	455.3	6.6	493	148	7.6
8974-56.1	66	51	0.793	6	5	0.001075	0.000447	0.0186	0.2682	0.0195	0.675	0.089	0.07723	0.00129	0.248	0.0634	0.0082	479.6	7.7	722	302	33.6
8974-57.1	90	47	0.537	7	5	0.000760	0.000897	0.0132	0.1934	0.0344	0.718	0.153	0.07582	0.00162	0.223	0.0687	0.0143	471.1	9.7	888	504	47.0
8974-60.1	281	201	0.738	23	9	0.000483	0.000272	0.0084	0.2167	0.0110	0.532	0.046	0.0739	0.00095	0.272	0.0522	0.0043	459.6	5.7	294	202	−56.3
8974-63.1	254	219	0.890	22	8	0.000500	0.000207	0.0087	0.2765	0.0106	0.561	0.037	0.07552	0.00103	0.326	0.0539	0.0034	469.3	6.2	367	147	−27.9
8974-66.1	159	225	1.465	16	6	0.000569	0.000226	0.0099	0.4509	0.0121	0.623	0.042	0.07555	0.00123	0.360	0.0599	0.0038	469.5	7.4	598	143	21.5
8974-67.1	534	458	0.887	46	10	0.000297	0.000116	0.0052	0.2669	0.0055	0.590	0.023	0.07588	0.0009	0.413	0.0564	0.0021	471.5	5.4	468	83	−0.8
8974-68.1	95	47	0.513	7	8	0.001247	0.000450	0.0216	0.1652	0.0184	0.562	0.076	0.07423	0.00127	0.248	0.0549	0.0073	461.6	7.7	408	328	−13.2
8974-69.1	155	81	0.542	12	8	0.000776	0.000250	0.0135	0.1665	0.0111	0.531	0.044	0.07346	0.00116	0.312	0.0524	0.0041	457.0	7.0	304	190	−50.4
8974-83.1	81	59	0.748	7	10	0.001895	0.000430	0.0329	0.2362	0.0186	0.590	0.077	0.07329	0.00147	0.275	0.0584	0.0074	456.0	8.8	546	302	16.5
8974-3.1	175	95	0.562	50	1	0.000036	0.000056	0.0006	0.1707	0.0043	3.411	0.092	0.2640	0.0048	0.760	0.0937	0.0017	1510.1	24.7	1502	34	−0.5
8974-35.1	164	112	0.706	31	9	0.000372	0.000128	0.0065	0.2096	0.0058	1.626	0.058	0.1711	0.0022	0.475	0.0690	0.0022	1017.9	12.2	898	67	−13.4
8974-65.1	56	25	0.460	5	8	0.001887	0.000807	0.0327	0.1258	0.0315	0.580	0.160	0.08794	0.00179	0.197	0.0479	0.0131	543.3	10.6	92	817	−491.6
8974-22.1	138	11	0.080	21	2	0.000088	0.000066	0.0015	0.0187	0.0026	1.682	0.047	0.16265	0.00274	0.693	0.0750	0.0015	971.5	15.2	1068	41	9.1
8974-14.2	132	66	0.515	24	14	0.000729	0.000114	0.0126	0.1531	0.0059	1.744	0.054	0.17242	0.00223	0.524	0.0733	0.0020	1025.4	12.3	1023	55	−0.2

Grain mount IP432; spot size 17 μm × 23 μm; no. of scans, 5; error in ^{206}Pb/^{238}U calibration, 1.1% (included).

Note: See Stern (1997). Spot name follows the convention *x-y.z*: *x*, sample number; *y*, grain number; *z*, spot number. Multiple analyses in an individual spot are labelled as *x-y.z.z*. Uncertainties reported at 1σ (absolute) and are calculated by numerical propagation of all known sources of error; $f(206)^{204}$ refers to mole percent of total ^{206}Pb that is due to common Pb, calculated using the ^{204}Pb method; common Pb composition used is the surface blank (4/6: 0.05770; 7/6: 0.89500; 8/6: 2.13840). Discordance relative to origin = 100[(207/206 age − 206/238 age)/(^{207}Pb/^{206}Pb age)]. Calibration standard 6266; U = 910 ppm; age = 559 Ma; ^{206}Pb/^{238}U = 0.09059.
* refers to radiogenic Pb (corrected for common Pb).

Table 4. Representative analyses of Buchans Group plutonic rocks.

Pluton/unit:	Wiley's Brook pluton		Little Sandy Lake pluton	Buchans River Formation granitoid cobbles							
Rock type[a]:	bt–hb gd	bt–hb gd	gd	Type 1 gd	Type 1 gd	Type 2 gd	Type 2 tn	Type 3 gd	Type 3 tn	Type 6 gd	Type 6 gd
Sample	RAX06	RAX06	VL06	RAX06	RAX06	RAX06	RAX06	RAX06	RAX06	RAX06	RAX06
Number	A186A	A187	45	A301-18	A301-15	A301-4	A301-5	A301-16	A301-12	A301-10	A301-11
UTM east:	499463	499628	524012	511074	511074	511074	511074	511074	511074	511074	511074
UTM north:	5402844	5402777	5408268	5408294	5408294	5408294	5408294	5408294	5408294	5408294	5408294
SiO_2 (wt.%)	75.70	76.35	73.00	77.24	77.45	74.86	78.43	80.35	79.67	66.69	67.48
TiO_2	0.22	0.25	0.38	0.44	0.42	0.55	0.24	0.19	0.13	0.80	0.88
Al_2O_3	12.96	12.93	13.75	12.46	12.51	13.54	11.49	11.60	11.10	16.54	16.33
Fe_2O_3	2.12	2.10	3.63	0.10	0.10	0.00	1.66	1.13	1.13	1.58	1.14
FeO	0.00	0.00	0.00	1.96	1.76	2.71	0.00	0.00	0.00	3.06	3.10
MnO	0.06	0.05	0.11	0.05	0.06	0.08	0.11	0.03	0.02	0.07	0.10
MgO	0.60	0.68	1.23	0.97	0.89	2.05	0.96	0.30	0.39	1.65	2.03
CaO	1.43	1.27	1.81	1.01	1.20	1.17	1.87	0.78	2.38	2.63	2.06
Na_2O	4.45	5.06	5.01	4.84	4.55	3.96	4.14	4.21	3.60	4.22	4.86
K_2O	2.40	1.26	0.99	0.87	1.00	0.99	1.07	1.40	1.56	2.50	1.57
P_2O_5	0.04	0.05	0.10	0.06	0.05	0.09	0.03	0.02	0.02	0.25	0.47
LOI	0.73	1.22	1.24	1.50	1.70	2.60	2.60	1.40	2.00	3.30	2.80
Total	100.73	101.22	101.24	101.50	101.70	102.60	102.60	101.40	102.00	103.30	102.80
Trace elements (ppm)											
Cr	35	14	12	<10	<10	<10	<10	<10	<10	<10	<10
Ni	9	8	5	<5	<5	<5	<5	<5	<5	<5	<5
Co	2	3	4	98	103	75	98	119	136	60	60
Sc	6.7	6.3	11.1	7.1	6.2	11.1	5.3	3.0	4.3	23.2	20.9
V	20	20	30	28	26	30	8	16	15	115	79
Cu	4	13	2	18	17	11	25	28	30	24	12
Pb	<1	<1	3	<1	<1	<1	<1	<1	<1	<1	<1
Zn	<5	<5	34	<5	<5	<5	<5	<5	<5	<5	<5
Cd	<0.1	<0.1	<0.1	0.6	1.0	0.8	0.6	0.5	0.6	0.7	0.9
Sn	1.2	0.9	0.7	<0.1	<0.1	<0.1	<0.1	<0.1	<0.1	<0.1	<0.1
W	0.2	0.4	0.2	<0.1	<0.1	<0.1	<0.1	<0.1	<0.1	<0.1	<0.1
Mo	0.9	1.2	0.4	<0.1	<0.1	<0.1	<0.1	<0.1	<0.1	<0.1	<0.1
Sb	0.1	0.1	0.2	1.3	1.9	0.3	0.6	0.8	1.4	1.4	1.7
Rb	56	21	15	12	16	16	18	24	24	32	23
Cs	2.2	0.7	0.4	0.2	0.3	0.6	0.4	0.2	0.3	0.8	0.6
Ba	814	465	384	602	700	769	2880	488	3370	1210	902
Sr	129	100	121	231	238	200	132	142	203	279	262
Tl	0.3	0.2	0.1	0.4	0.6	0.4	0.3	0.5	0.8	1.2	0.9
Ga	11.8	11.4	12.5	10.8	10.8	11.7	9.7	8.5	7.4	16.0	15.9
Li	15.3	18.2	3.9	<0.5	<0.5	<0.5	<0.5	<0.5	<0.5	<0.5	<0.5
Ta	0.31	0.28	0.28	0.83	0.77	0.77	0.86	0.93	1.02	0.56	0.53
Nb	4.6	4.2	4.2	5.3	4.5	4.9	5.7	5.4	6.3	4.1	3.8
Hf	3.0	3.5	3.2	4.1	3.7	4.4	4.7	3.8	3.1	3.1	2.7
Zr	96	113	117	151	135	164	164	112	95	109	98
Y	25	21	20	22	17	20	23	21	18	19	22
Th	8.3	6.7	6.1	9.8	9.1	9.2	11.4	13.4	12.2	6.4	6.0
U	1.4	1.6	1.6	2.6	1.9	2.6	2.7	3.2	1.7	1.9	2.3
La	26.7	19.1	18.0	33.1	25.1	30.1	35.5	32.3	30.9	18.6	43.4
Ce	52.8	37.5	35.1	65.7	49.7	58.2	70.0	63.0	60.1	38.9	85.5
Pr	6.0	4.4	4.0	7.5	5.6	6.6	7.8	6.9	6.3	4.8	9.4
Nd	22.2	16.4	15.2	28.0	20.0	24.2	27.9	24.8	21.9	19.2	34.5
Sm	4.4	3.4	3.2	5.4	3.8	4.6	5.1	4.3	3.8	4.1	6.2
Eu	0.72	0.67	0.80	1.12	1.10	0.85	0.89	0.74	0.64	0.87	1.20
Gd	4.07	3.33	3.28	4.68	3.28	3.86	4.13	3.53	3.02	3.87	5.28
Tb	0.66	0.55	0.52	0.72	0.51	0.60	0.66	0.55	0.49	0.58	0.77
Dy	4.32	3.69	3.38	4.04	3.00	3.52	4.00	3.43	2.92	3.52	4.22
Ho	0.92	0.79	0.73	0.82	0.63	0.75	0.85	0.77	0.64	0.72	0.86
Er	2.86	2.50	2.22	2.44	1.93	2.26	2.65	2.42	2.00	2.11	2.49
Tm	0.44	0.40	0.34	0.37	0.31	0.35	0.42	0.39	0.33	0.32	0.36
Yb	3.05	2.83	2.35	2.60	2.14	2.36	3.01	2.79	2.31	2.08	2.36
Lu	0.48	0.46	0.37	0.43	0.35	0.39	0.51	0.47	0.38	0.33	0.38
Be	1.28	1.29	1.11	1.13	1.03	0.94	0.62	0.82	1.03	4.22	1.45
La/Sm	6.1	5.5	5.6	6.1	6.6	6.6	6.9	7.5	8.0	4.5	7.0
La/Yb	8.8	6.7	7.6	12.7	11.7	12.7	11.8	11.6	13.4	9.0	18.4
Mg#[b]	24.0	26.4	27.4	32.1	32.4	43.1	39.2	22.7	27.8	27.0	32.9

[a]Rock type names derived from Fig. 3. Abbreviations: bt, biotite; hb, hornblende; gd, granodiorite; tn, tonalite.
[b]Mg# = 100[MgO/(FeO^{total} + MgO)].

Fig. 3. Buchans granitoid cobbles and the WBG and LSLG plotted on the CIPW normative Q′ (100[Q/(Q + Or + Ab + An)]) versus ANOR (100[An/(Or + An)]) classification diagram (Streckeisen and Le Maitre 1979). Also shown are (*i*) the trend for an Oligocene strongly calcic intraoceanic arc plutonic suite (labelled NB; based on data of Whalen (1985)) and (*ii*) compositional trends for different representative types of plutonic suites from Whalen and Frost (2013) (A, alkalic; A-C, alkali-calcic; C-A, calc-alkalic; C, calcic).

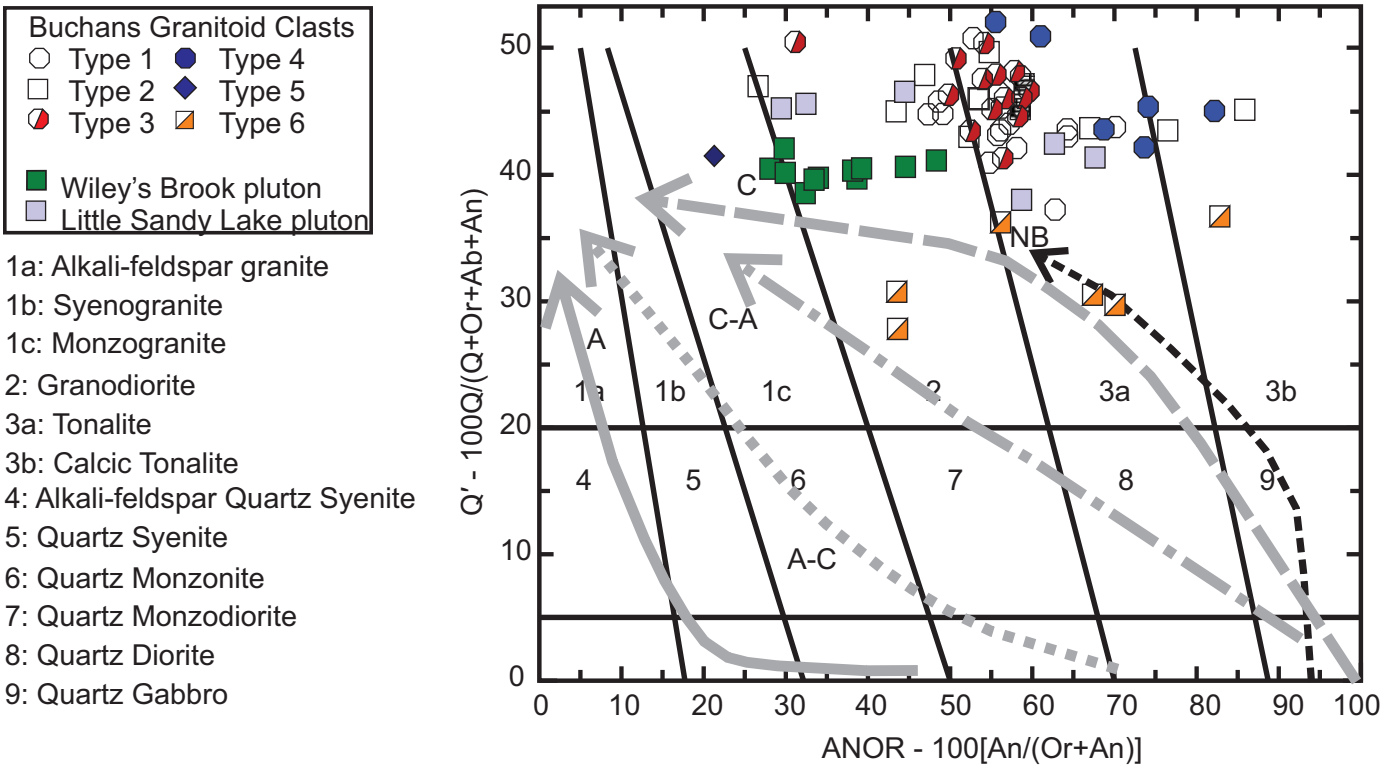

(Fig. 7). Based on their higher Sr, P, and Ti contents, Type 6 cobbles and the LSLG were derived from a less evolved magma than the WBG and other cobble types (Fig. 7*d*). Lower Rb and K within Type 1–3 cobbles and the LSLG than the WBG may reflect alkali element mobility due to hydrothermal alteration. Based on their higher Th and lower P and Ti contents, Type 3 cobbles probably crystallized from a more evolved magma than the other sample types.

Based on WBG normalized patterns in Fig. 7, (*i*) enrichment of the Oriental rhyolite in La through Lu is compatible with it being less evolved than the WBG; (*ii*) the MacLean dacite and Clementine rhyolite are depleted in Y and heavy rare-earth elements, suggesting they are not co-genetic with the WBG; (*iii*) one Clementine rhyolite sample is enriched in P and Ti, suggesting a less evolved character than the WBG; and (*iv*) overall similarities between Type 1 and 2 cobbles and Clementine samples suggest they may be co-genetic and not closely related to the WBG. When comparing and distinguishing between different Middle Ordovician volcanic units within the AAT, immobile element ratios such as Th/Nb, Nb/La, La/Sm, and La/Yb are particularly useful. Buchans Group felsic units can be subdivided based on La/Sm and La/Yb ratios into Felsic 1 (9.10 ± 1.63 and 13.6 ± 3.0) (MacLean dacite and Clementine rhyolite units) and Felsic 2 (4.69 ± 0.80 and 7.1 ± 1.9) (Oriental rhyolite) groups (e.g., van Hees 2011). Based on La/Yb values (see Table 4), 13 of 17 granitoid cobbles collected from the Old Buchans exposure fall within the Felsic 1 group, whereas the other cobbles and the WBG correspond to the Felsic 2 group. In regard to La/Sm values, nine cobbles lie between 5.5 and 7.5, intermediate between the two groups. This highlights the close coincidence in characteristics between Buchans Group extrusive and plutonic lithologies.

Nd isotopes

Nd isotopic analyses of the WBG and LSLG and Buchans Group granitoid cobble types, calculated for ε_{Nd} (*T*) (*T*, time of crystallization) values at 465 Ma and depleted-mantle model (T_{DM}) ages are presented in Table 5 and shown in Fig. 8. Four granitoid cobble ε_{Nd} (*T*) determinations (–1.95 to –4.0) fall within or very close to the range obtained from VMS-related felsic volcanic units of the Buchans Group (–2.04 to –3.84; Table 5). The ε_{Nd} (*T*) value of –2.97 obtained for the LSLG also falls within this range, but the –0.95 value yielded by the WBG is distinctly less negative. The ε_{Nd} (*T*) range obtained from Buchans Group felsic igneous units is more restricted and less negative than typical Ordovician plutonic samples elsewhere in the Notre Dame subzone (Fig. 8; ε_{Nd} (465 Ma) one sample at +0.60, 17 samples at –1.13 to –13.60, Whalen et al. 1997) suggesting an isotopically more homogeneous source.

Discussion

Buchans Group volcanic rocks that host VMS deposits have been characterized as a calc-alkaline suite generated within a continental arc setting (e.g., Swinden et al. 1997). In keeping with this interpretation, both cobble and plutonic samples are classified as arc-type granitoids on the various trace-element tectonomagmatic discrimination diagrams of Pearce et al. (1984) (not shown). Negative Nb and Ti anomalies that these granitoid samples exhibit on extended-element normalized plots (Fig. 6) are compatible with, but not diagnostic of, an arc setting. WBG and LSLG plutonic samples are depleted in large-ion lithophile elements (LILE) and high-field-strength elements (HFSE) (Fig. 6) compared with "typical" continental magmatic arc granitoid rocks (Tarney and Jones 1994), and they exhibit ratios of Rb/Sr and Rb/Zr that are mainly <0.15 and <0.8, respectively. These features, along with being magnesian (oxidized) and calcic (Fig. 4), are characteristic of

Fig. 4. Buchans granitoid cobbles and WBG plus LSLG samples plotted on the (*a*) $FeO^{total}/(FeO^{total} + MgO)$ (or Fe*) versus SiO_2 and (*b*) $Na_2O + K_2O - CaO$ (or MALI) versus SiO_2 granitic rock classification diagrams of Frost et al. (2001). In *a*, the boundary between ferroan and magnesian plutons has been modified, as suggested by Frost and Frost (2008). The trend for an Oligocene strongly calcic intraoceanic arc plutonic suite is labelled NB (based on data of Whalen (1985)). Shown in *b* are ranges for alkalic-calcic, calc-alkalic, and calcic rock series, based on the alkali-lime classification of Peacock (1931). However, based on the mainly low MALI values of most of our samples, the calcic range has been further subdivided into fields labelled A–C.

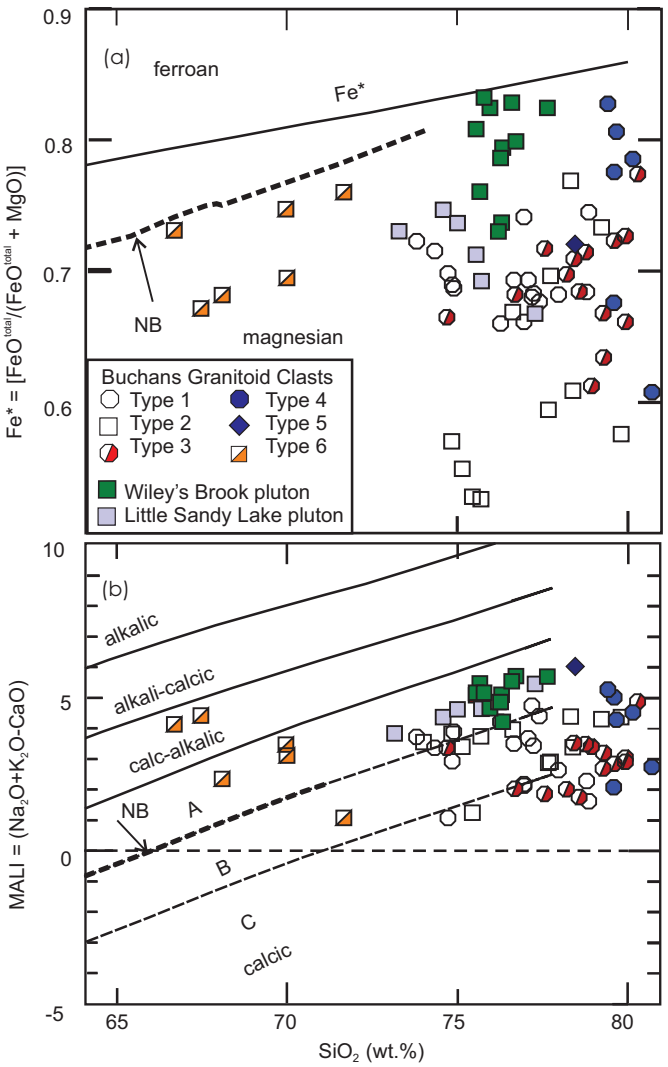

primitive arc plutonic rocks (Figs. 3 and 4; Whalen 1985; Chappell and Stephens 1988; Tarney and Jones 1994).

Overall, major and trace element features, and isotopic characteristics, suggest that the pluton(s) that sourced the cobbles displayed both textural and geochemical diversity. For example, Type 6 cobbles are distinctly less evolved than all other cobble types, whereas Type 3 cobbles are more evolved (higher Th and lower P) than other granitic and aplitic cobble types. Based on observations of the Buchans River Formation made in underground drifts and in drill core, Stewart (1987) and Binney (1987) identified temporal changes in cobble type, abundance, and morphology. Deposition of the less-evolved Type 6 cobbles predates coarse-grained granitic cobble types, and both mainly predate fine-grained aplitic cobble types. Regardless of the genetic models for formation of cobbles, the temporal changes in deposition of cobbles indicate that the source changed over time.

Thurlow and Swanson (1987) and subsequent workers (e.g., van Hees 2011; van Hees et al. 2012) have divided felsic volcanic rocks in the Buchans area into at least two different types. Geochemical studies indicate that felsic volcanic rocks are characterized by distinct La/Sm and La/Yb ratios, suggesting different sources and (or) different pressure (*P*) and temperature (*T*) conditions of melting (e.g., van Hees 2011). Granitoid cobbles at the Old Buchans exposure have a similar variation in these ratios, indicating that both Buchans Group extrusive and plutonic lithologies were derived from similarly diverse parent magmas or sources.

Geochemical, U–Pb geochronological, and Nd isotopic results are compatible with plutonic (granitoid cobbles) and VMS-hosting extrusive (Clementine rhyolite, MacLean dacite, and Oriental rhyolite) units within the Buchans Group forming from at least two temporally equivalent magma types. Plutonic and volcanic rocks in each of these magma types may be genetically related, either through fractional crystallization or partial melting of similar protoliths under comparable *P*–*T* conditions. The multiple magma types may have coexisted within the same magma chamber or at different depths. Moreover, these magmas could have formed zoned or polyphase hypabyssal pluton(s).

Stewart (1987) noted that finer-grained cobble types were cut by pre-entrainment quartz + calcite + barite ± sulfide-filled fractures and that the coarser-grained cobble types were pervasively hydrothermally altered prior to rounding. Thus, solidification, fracturing, veining, and hydrothermal overprinting predated cobble incorporation into debris flows. These features suggest that the various granitoid cobble types were derived from a hypabyssal system that was associated with, or affected by, significant hydrothermal activity. Alternatively, the cobbles may have been erupted on the sea floor proximal to VMS-generating hydrothermal vents where they were altered prior to transport to their present location along with reworked ore. This latter interpretation is more in keeping with the argument of Stewart (1987) that the LSLG and WBG, which do not exhibit such hydrothermal alteration, represent the hypabyssal sources for cobbles in the Buchans orebodies.

Are the exposed plutons the source of cobbles?

The LSLG is a small, hypabyssal pluton with an apparent volcanic carapace consisting of columnar jointed rhyolite and breccia. In general, the geochemistry of the LSLG indicates that it is more primitive than the WBG and most of the cobbles sampled by the Old Buchans conglomerate. Thurlow and Swanson (1981, 1987) interpreted the LSLG to intrude into a separate thrust slice above the Airport Thrust (see Fig. 1). Subsequent studies demonstrated that the LSLG intrudes into a distinct, predominantly tholeiitic structural panel (e.g., Zagorevski and Rogers 2009) consistent with its more primitive composition. Because the LSLG lies in a distinct structural slice and has unique host lithologies, it is unlikely to represent the source of the granitoid cobbles.

Similar to the LSLG, the WBG forms a subvolcanic pluton with apparent hypabyssal phases and minor volcanic breccia. Overall, the geochemistry of the WLG is similar to Buchans Group cobbles and volcanic rocks; however, the WBG appears to be more evolved or derived from a different source from at least some of the cobble types. This difference is highlighted by a distinctly more juvenile ε_{Nd} value for the WBG than for the felsic volcanic rocks or cobbles (Table 5). These differences suggest that the WBG was not the source of the cobbles at the Old Buchans conglomerate.

Our geochemical and isotopic data demonstrate that, in contrast to Stewart (1987), the exposed LSLG and WBG are unlikely to be the direct hypabyssal sources for cobbles in the Buchans orebodies. Sourcing the cobbles from LSLG and WBG hypabyssal systems would require the following assumptions that are not supported by data: (*i*) these plutons are zoned and formed by

Fig. 5. FeO^{total} versus various major- and trace-element plots for Buchans granitoid cobbles and WBG plus LSLG samples. FeO^{total} is employed as the *x* axis in these Harker diagram-like plots, as hydrothermal alteration of granitoid cobble samples has introduced secondary quartz (see Fig. 3 and text). Key to symbols shown in legend.

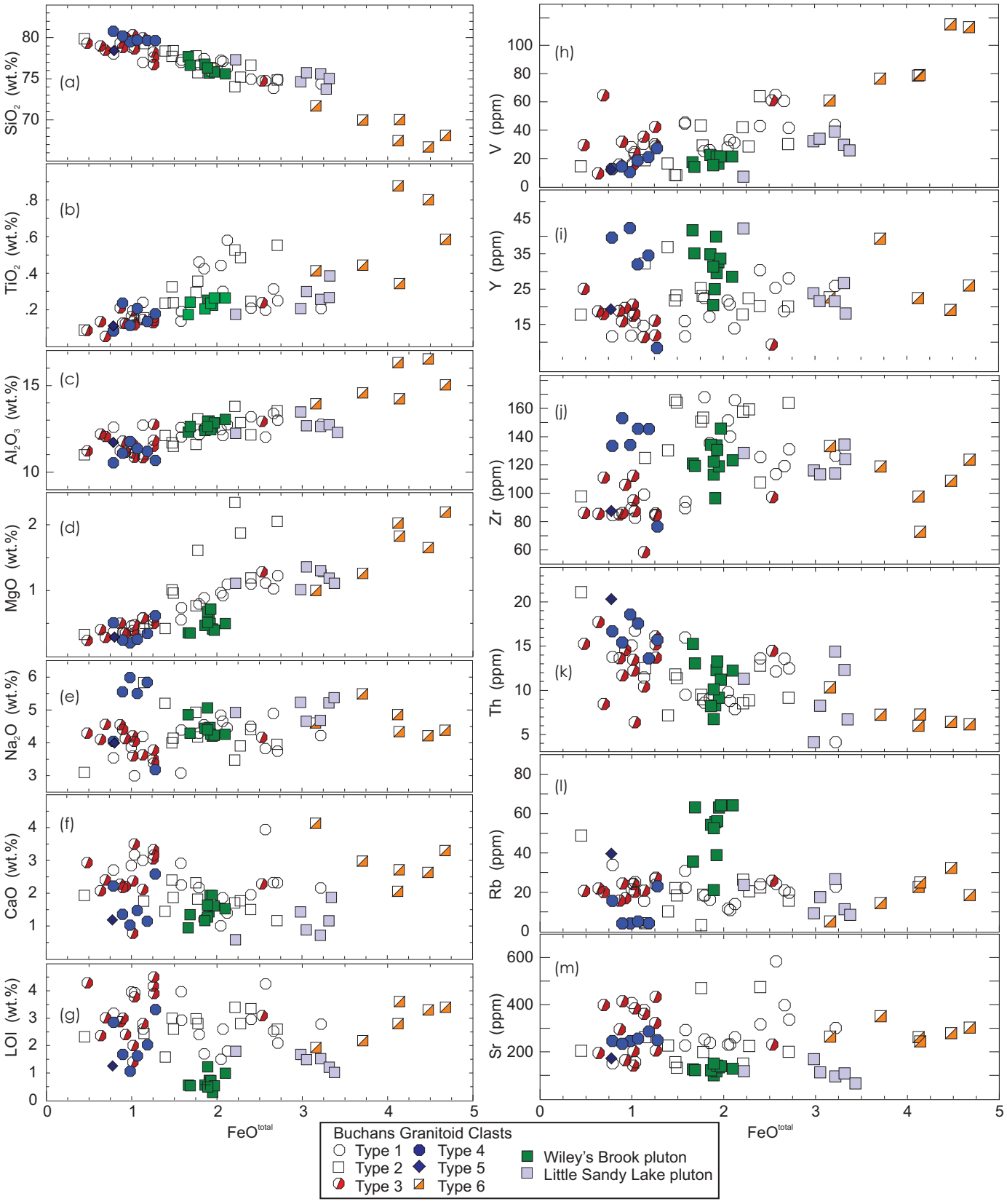

Fig. 6. Primitive mantle-normalized extended-element plots for samples (*N*) from (*a*) the WBG and LSLG plutons, (*b–e*) Buchans granitoid cobble types, and (*f*) average compositions of Buchans Group felsic volcanic units (data from Zagorevski and Rogers 2011). Because of the presence of hydrothermal barite, Ba is not plotted for granitoid cobble and volcanic samples. Normalizing values are from Taylor and McLennan (1985). Ba excluded owing to the presence of hydrothermal barite.

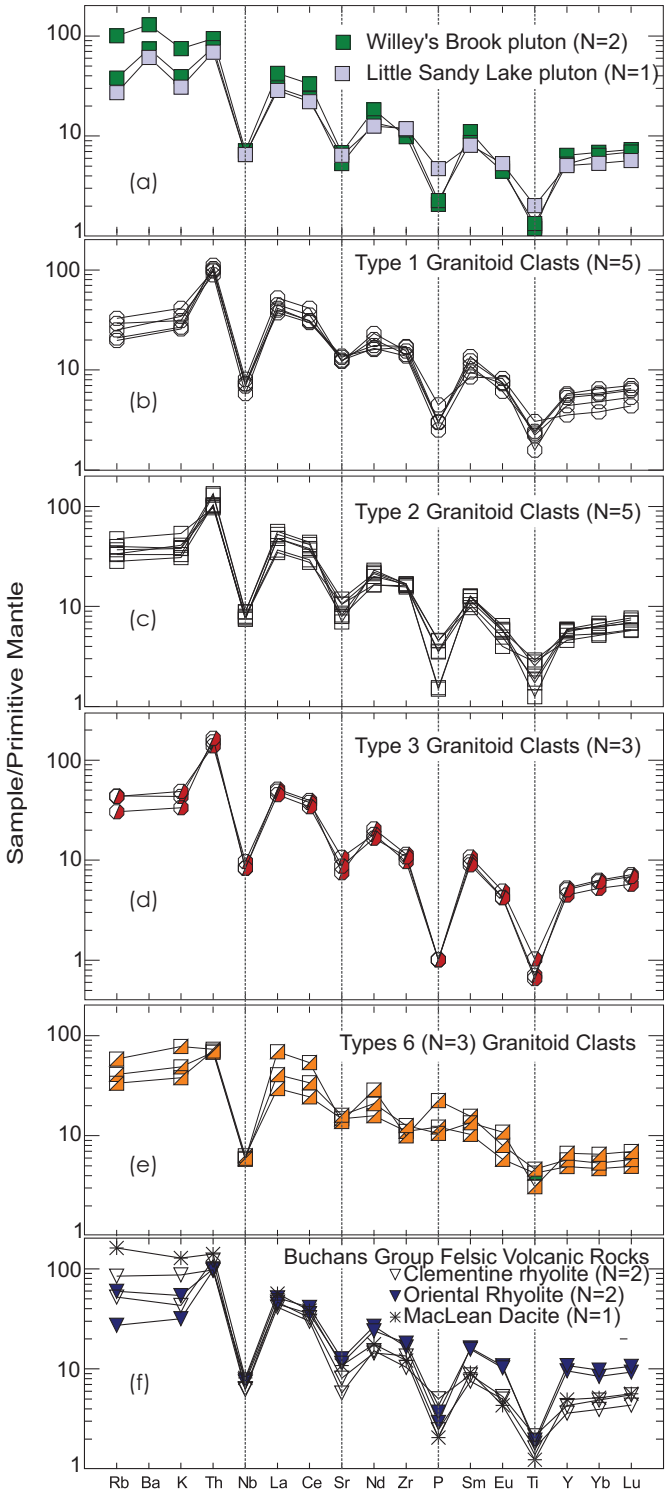

Fig. 7. WBG normalized extended-element plots for (*a–d*) samples of Buchans granitoid cobble types and (*e*) the LSLG and Buchans Group felsic volcanic units. These plots facilitate comparison of these felsic intrusive rock compositions and evaluation of a possible co-magmatic relationship between them (see text).

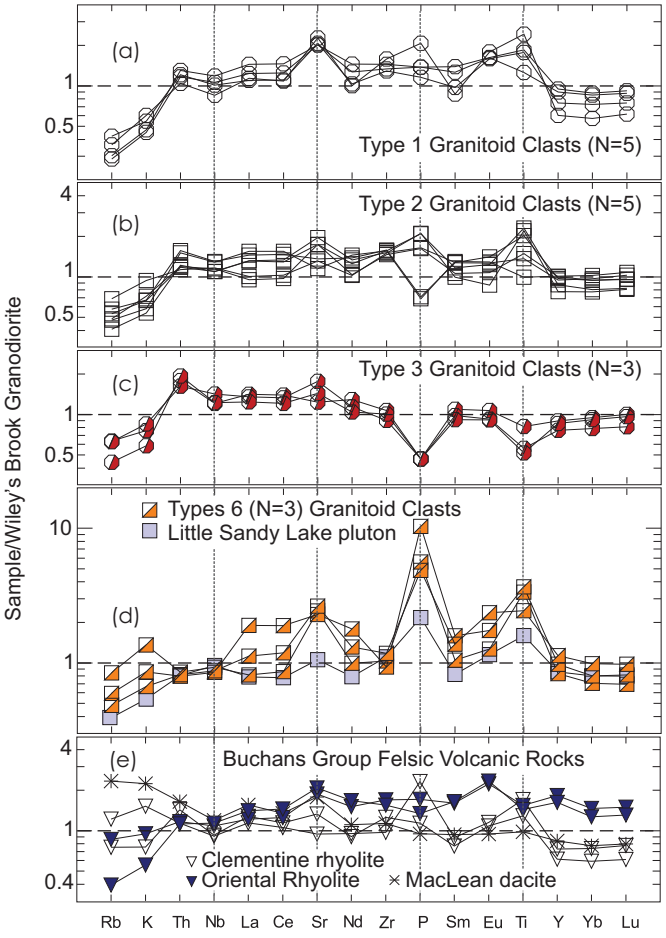

intrusion of several discrete and distinct magma batches; (*ii*) the plutonic phases that were the source of the cobbles are not exposed or preserved; and (*iii*) the exposed plutonic phases escaped the intense hydrothermal alteration that is seen in the cobbles.

How did the cobbles form?

The highly rounded granitoid cobbles form a major component within debris flows in the Buchans VMS orebodies. Two significantly different models have been proposed to account for the rounding of the granitoids relative to volcanic, sedimentary, and sulfide fragments. The first model proposes that the cobbles were rounded and transported to surface by explosive hydrothermal activity in breccia pipes that originated within an exsolving hypabyssal pluton that was syn-genetic with VMS deposition. The alternative model has the cobbles derived by subaerial erosion of an emergent plutonic island fringed by a granitoid cobble beach. Irrespective of the cause of the rounding, both models require downslope transport and mixing of granitoid cobbles and other lithologies within debris flows (Binney 1987).

Stewart (1987) proposed a model involving rounding and emplacement of granitoid cobbles via breccia pipes based on observations of the Buchans River Formation made in underground drifts and in drill core. The evidence for this model includes temporal changes in cobble type, abundance, and morphology. These were interpreted by Stewart (1987) as sampling successive stages

Table 5. Nd isotopic analyses of volcanic and granitoid rocks from western Newfoundland.

Sample No.	Lithology[a]	UTM east	UTM north	SiO_2 (wt.%)	U–Pb age (Ma)	ε_{Nd} (465 Ma)	T_{DM}[b] (Ga)	$^{143}Nd/^{144}Nd$ (m)	$^{147}Sm/^{144}Nd$ (m)	Nd (ppm)	Sm (ppm)
RAX06A301-19	Tonalite cobble Type 1	511074	5408294	76.7	—	−1.95	1.03	0.512217	0.0913	19.58	2.96
RAX06A301-5	Tonalite cobble Type 2	511074	5408294	78.4	—	−3.79	1.27	0.512181	0.1104	25.92	4.73
RAX06A301-8	Tonalite cobble Type 3	511074	5408294	80.0	—	−4.01	1.27	0.512163	0.1082	17.94	3.21
RAX06A301-10	Granodiorite cobble Type 6	511074	5408294	66.7	—	−4.07	1.50	0.512230	0.1311	16.62	3.60
RAX06A186 A	Wiley's Brook granodiorite	499463	5402844	75.7	466.7±0.5[c]	−1.00	1.19	0.512379	0.1284	18.30	3.89
VL06045	Little Sandy Lake tonalite	524012	5408268	73.0	—	−2.97	1.37	0.512279	0.1288	15.31	3.26
RAX06A296	Rhyolite south of Lucky Strike	509436	5406632	73.4	—	−2.04	1.60	0.512370	0.1430	15.59	3.69
RAX07A527	MacLean orebody rhyolite	508428	5408871	67.7	463±4[d]	−3.84	1.31	0.512154	0.1024	18.65	3.16
WX89NF-25	Woodsfords Arm monzogranite	580400	5485700	76.5	464±3[d]	−1.53	1.08	0.512282	0.1056	20.13	3.56
VL01A081	Otter Pond granodiorite	447005	5341785	71.1	468±2[e]	−6.80	1.63	0.512063	0.1222	20.83	4.21
WXNF-33	Hungry Mountain complex tonalite	536200	5465100	71.4	—	0.60	1.21	0.512519	0.1476	9.63	2.35
WXNF-34	Hungry Mountain complex tonalite	527900	5458400	70.8	—	−7.07	1.70	0.512060	0.1257	15.00	3.13
WXNF-48	Hungry Mountain complex tonalite	540400	5434700	67.0	463±3[f]	−5.96	1.89	0.512172	0.1436	19.97	4.74
WXNF-95	Hungry Mountain complex tonalite	512200	5452600	66.5	—	−10.04	2.14	0.511935	0.1346	13.48	3.00
WXNF-96	Hungry Mountain complex tonalite	529000	5453800	68.6	—	−4.55	1.65	0.512229	0.1389	9.86	2.27

[a]Plutonic rock types based on Q′–ANOR diagram of Streckeisen and Le Maitre (1979) (see Fig. 2).
[b]Depleted mantle ages (T_{DM}) based on model of DePaolo (1981).
[c]From this paper.
[d]From Zagorevski and McNicoll, unpublished data.
[e]From Lissenberg et al. (2005).
[f]From van Staal et al. (2007).

Fig. 8. ε_{Nd} (465 Ma) values for the WBG and LSLG, granitoid cobble types, and Buchans Group VMS-related felsic volcanic units. The ε_{Nd} (465 Ma) range for Notre Dame arc plutons from the adjacent Notre Dame subzone is shown for comparison (data from Whalen 2012).

of an evolving subsurface magmatic system via explosive breccia pipes. In this model, hydrothermal alteration and veining of granitoid cobbles prior to their rounding supports an evolving magmatic-hydrothermal system.

Extensive hydrothermal brecciation is common in Buchans stockwork zones, including jigsaw fit of host basaltic andesite and rhyodacite flows (van Hees et al. 2012); however, brecciation appears to be restricted to the altered host lithologies, and exotic, granitoid fragments have not been observed (van Hees 2011). The hypothesized breccia pipe is nowhere exposed; thus, if it existed, it would have had to close following "eruption" of granitoid cobbles and be completely eroded or hidden by thrust faults (cf. Stewart 1987). Thurlow and Swanson (1981) compared the breccia pipe model with pebble dykes associated with Kuroko deposits. Similar pebble dykes have been identified at Buchans (Thurlow 2001); however, these do not seem to be viable analogues, because the mean clast diameter of the Buchans granitoid clasts (17.1 × 10.6 cm, $n = 70$: Stewart 1987) greatly exceeds the maximum size of pebbles in the post-ore pebble dykes that cut the Kuroko deposits (<8 cm; T. Urabe, personal communication 2013).

Clast sizes and morphology similar to Buchans cobbles have been documented in other magmatic-hydrothermal systems, such as within giant copper porphyry deposits, where they are intimately associated with ore (e.g., El Tiniente deposit, Chile; plate 15 in Taylor 2009). However, these are more typical for phreatomagmatic explosive activity, as opposed to the phreatic eruption associated with the Kuroko deposits (see Sillitoe 1985). Similarly sized granite blocks can also be produced by in situ milling during phreatomagmatic brecciation (e.g., Black Range dolerite dyke, Western Australia: van Kranendonk et al. 2006). However, this situation is not directly analogous to the scenario proposed by Thurlow and Swanson (1981) and Stewart (1987) in that these granite blocks are demonstrably incidental fragments of country rocks and are associated with chilled melt droplets.

In a review of hydrovolcanic breccia pipe structures Tămaş and Milési (2002) identified several instances where rounding of clasts occur. Indeed they state that although clasts range from angular to well rounded, the rounded forms are the most common. Typically, it is the smaller clasts that are more well rounded, as these have undergone the most intense working (milling and abrasion) in the fluidized breccia zones within a hydrovolcanic pipe or diatreme (normally the central portion of the pipe). These observations are in contrast to Buchans, where it is the granitoid clasts that are the largest and large vertical transport is not expected. An alternative "hypogene exfoliation" model for rounding of large clasts in vent breccias was proposed by Farmin (1937). In this case, the rounding occurs owing to thermal shock, causing exfoliation

along closely spaced concentric fractures. Sillitoe (1985) suggested that this was the mechanism for the rounding of the Buchans granitoid cobbles, even though the characteristic concentric fracturing was not recorded.

Implicit in the Stewart (1987) model is that the rounding and grading (or sorting) of granite clasts were achieved by attrition as the blocks were sorted by neutral buoyancy within the vent. This scenario is highly unlikely because, irrespective of the vent dimensions, a zone of neutral buoyancy would likely rapidly block the vent, either causing a cessation of the system or overpressurization, resulting in explosive evacuation of the collapsed vent.

The alternative model for the formation of the Buchans granitoid cobbles has them formed by subaerial or shallow marine erosion of an emergent island fringed by a granitoid cobble beach. This model requires (*i*) discrete subvolcanic systems or phases within error of our geochronology; (*ii*) several ages of alteration and mineralization (economic or not); (*iii*) emergent island(s) coeval with the observed predominantly submarine volcanism and VMS formation; (*iv*) isolated sources of several distinct cobble types; (*v*) mass wasting from multiple sources into a single basin.

Modern intraoceanic volcanic centres

Since the development of the genetic models of Buchans ore deposits, extensive multi-beam mapping and sampling of submarine volcanic centres and associated VMS mineralization have been carried out. This effort has resulted in an improved understanding of the morphology and stratigraphy of volcanic centres and submarine calderas (e.g., Hekinian et al. 2008; Graham et al. 2008; Stern et al. 2008; Tani et al. 2008), preponderance of hydrothermal venting around active volcanic centres (e.g., de Ronde et al. 2001, 2005; Stoffers et al. 2006; Graham et al. 2008), the influence of marine low-stand conditions on formation of submerged submarine terraces (e.g., Le Friant et al. 2004; Leat et al. 2010), and the importance of mass wasting in both submarine and emergent volcanic centres (e.g., Leat et al. 2010; Tani et al. 2008). This section will review some of the features of modern and recent island arc volcanic centres and relate them to the interpretation of the Buchans Group.

Many modern volcanic centres display a complex evolution that is characterized by several stages of magmatism and caldera formation (i.e., seven nested calderas in the Hinetapeka volcanic centre in the Kermadec arc: Graham et al. 2008). In such circumstances the resultant caldera wall scarps can expose up to 1 km of relief (Graham et al. 2008; Stern et al. 2008; Tani et al. 2008). Caldera walls typically expose voluminous volcanic and volcaniclastic material, along with subvolcanic intrusions (e.g., Hekinian et al. 2008; Stern et al. 2008; Tani et al. 2008). Locally, extensional faults also expose older volcano-plutonic basement (Graham et al. 2008). Locally emergent islands along the caldera rim can expose pre-caldera volcanic and hypabyssal systems, such as at Sumisu (fig. 2 in Tani et al. 2008). Evidence for at least some hydrothermal activities are apparent for most volcanic centres, ranging from high-temperature sulfide vents to cool mussel beds (e.g., de Ronde et al. 2001, 2005; Stoffers et al. 2006; Graham et al. 2008). Many volcanic centres have more than one hydrothermal discharge site (Stoffers et al. 2006; Graham et al. 2008), and there is evidence for pre-caldera hydrothermal alteration in the caldera walls (e.g., Stern et al. 2008).

Emergent islands along caldera rims can be coeval with predominantly submarine volcanism and VMS formation along the caldera floor or along volcanic flanks (e.g., Sumisu: Tani et al. 2008). Such islands are often flanked by cobble to boulder beaches derived from active volcanic centres (Leat et al. 2010) or pre-caldera lithologies (Tani et al. 2008). Small islands represent isolated sources for cobble beach formation and, in many cases, these beaches are overrepresented by resistant lithologies. For example, Sumisu Island exposes scoria, lava flows, and abundant hypabyssal intrusions (Tani et al. 2008). Although the composition of the beach boulders and cobbles have not been studied in detail, more resistant hypabyssal intrusions are likely to be overrepresented in the clast population relative to scoria. Submerged caldera walls also locally preserve beach cobbles (Stern et al. 2008), demonstrating submergence due to relative sea-level change (either global or local in response to inflation or deflation of volcanic edifice). Additionally, many volcanoes display shallow shelves, interpreted to represent erosion surfaces formed during the last glacial maximum and low-stand sea level (Leat et al. 2010) and (or) erosion above effective storm wave base (Graham et al. 2008; Ishizuka et al. 2002)). As with emergent islands, these shelves are expected to be dominated by resistant clasts that are derived from the eroded volcanic carapace and its hypabyssal feeder system. Following erosion at or near sea level, sedimentary and volcaniclastic material is transported downslope to the flanks of the volcano and (or) into the caldera. Transport takes place by mass flows along sediment chutes and as large-scale slides and debris flows (e.g., Leat et al. 2010). The source area of debris and thus lithologies that are transported in sediment chutes can be very restricted. For example, in the South Sandwich arc, many sediment chutes originate from shallow, erosional shelves around islands (Leat et al. 2010).

Comparison of Buchans Group to modern volcanic environments

This section will examine whether the caldera model for the Buchans area developed by Thurlow (1977, 1981*b*); Thurlow and Swanson (1981), and Kirkham and Thurlow (1987) explains all the features observed in the Buchans orebodies by applying typical volcano-sedimentary processes observed in modern island arc volcanic centres. As discussed earlier in the text, modern island arc volcanic centres are frequently characterized by calderas, whether formed singularly or as nested multiple events. The age differences between pre-, syn-, and post-caldera lithologies, and related hydrothermal alteration in modern environments (e.g., ~0.5 Ma for exposed lithologies in the West Rota volcano; Stern et al. 2008), are well within geochronological constraints for the Buchans area. Furthermore, the evidence for multiple volcanic (van Hees 2011) and plutonic magma types (see earlier in the text) does not necessitate that Buchans formed as a single, large, evolving volcano-plutonic system as proposed by Stewart (1987). Although polyphase deformation hampers interpretations of primary volcano-sedimentary architectures in ancient environments such as Buchans (e.g., Calon and Green 1987), the diverse magmatism, rapid facies variations, and abrupt changes in unit thickness are suggestive of the significant topographic relief coeval with magmatism that would be expected in a caldera-like environment (Fig. 9).

Modern caldera walls expose extensive cross sections of volcano-sedimentary stratigraphy, including locally significant hypabyssal intrusions and pre- to syn-caldera hydrothermal alteration. The alteration of granitoid and "other" type hypabyssal cobbles described by Stewart (1987) could easily have been derived from pre-caldera lithologies exhumed during caldera formation. Caldera collapse can occur along zones weakened by metasomatic alteration associated with hydrothermal processes (Siebert 1984; Leyrit 2000; Clément et al. 2002). Such a scenario could explain the preponderance of pre-entrainment alteration observed within the granitoid and aplitic cobbles (Stewart 1987).

Derivation of cobbles through subaerial erosion was not favoured by the Stewart (1987) model because there was no known subaerial arc magmatism in the Buchans area, and the debris flows exhibit a temporal change in source magma type. Recent volcanic regions demonstrate that emergent volcanic systems can have limited preservation potential in the geologic record, because they are exposed to subaerial erosion (i.e., strong wave action, chemical weathering, etc.) as exemplified by Sumisu Island (Tani et al. 2008) and Manji Seamount (Ishizuka et al. 2002). Thus, the absence of clear evidence for subaerial magmatism should not

Fig. 9. Schematic setting of the Buchans area (modified from Kirkham and Thurlow 1987): A, discrete emergent islands with cobble beaches expose pre-caldera or rift hypabyssal rocks of different ages or phases; B, shallow submarine shelves are formed as a result of erosion by storm wave action, low-stand sea level, and (or) subsidence of a subareal volcanic centre; C, pre-caldera or rift volcanic and hypabyssal rocks are exposed in fault scarps; D, debris flows and slides sample different sources at different times, resulting in apparent temporal changes in clast types; E, active hydrothermal system deposits massive sulfides; F, transported ores are formed by mass wasting from active hydrothermal sites; G, transported ore debris flows remobilize and incorporate previous debris flows, resulting in apparent temporal change downslope.

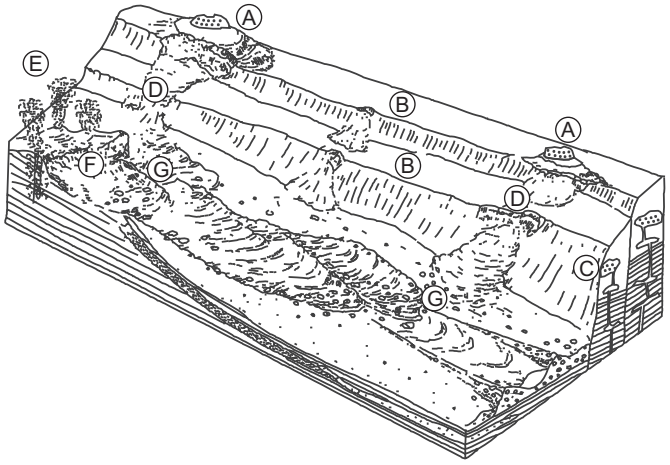

be used to discount the possibility of emergence of volcanic centres. Even in recent volcanic centres, low-stand sea levels have resulted in extensive erosion of volcanic centres (Le Friant et al. 2004; Leat et al. 2010). Similar rapid changes in global sea level, including extreme low-stand conditions, have been recognized in the Middle Ordovician (Ainsaar et al. 2010; Keller and Lehnert 2010; Munnecke et al. 2010; Videt et al. 2010), although chronological controls of Buchans Group events are insufficiently precise to correlate definitively with global sea-level fluctuations. Even though evidence for subaerial magmatism and erosion is very sparse in central Newfoundland, there are extensive breccia–conglomerate units in most Darriwilian terranes throughout the AAT (Bostock 1988; Zagorevski and van Staal 2011; Coombs et al. 2012) and unconformities on older arc basement (Robert's Arm Group; Zagorevski and McNicoll, unpublished data). These observations support emergence of Darriwilian volcanic arc centres, possibly driven by global low-stand conditions and (or) by regional tectonic effects. Hence, the presence of predominantly submarine volcanism associated with Buchans VMS ores does not exclude emergence of parts of the pre-caldera volcanic systems along relative topographic highs, such as caldera rims (Fig. 9).

Emergence of subaerial volcanic centres, exhumation of pre-caldera volcanic–hypabyssal systems along the caldera walls or rim, and eustatic sea-level changes can all contribute to formation of cobble to boulder beaches. The rapid erosion of intraoceanic islands tends to concentrate beach cobbles to resistant lithologies that are exposed in these islands. Subsequent downslope transport (i.e., into a caldera) of these erosion products through sediment chutes can easily result in input of different lithologies over time. Hence, the apparent temporal change in cobble types explained in terms of a breccia pipe model by Stewart (1987) can equally well be explained by erosion of locally emergent sections and in this latter case does not require circumstances that are not commonly observed in analogous modern volcanic systems.

Conclusions

Buchans VMS orebodies are characterized by a distinctive association of ore with rounded granitoid cobbles. Data on these granitoid cobbles and exposed Buchans-area plutonic rocks indicate that the cobbles and plutonic rocks display subtle but important geochemical and isotopic differences. Similar differences have been documented in associated volcanic rocks (van Hees 2011; van Hees et al. 2012). The ages obtained from the volcanic, plutonic, and sedimentary rocks suggest that all were broadly coeval, within error of geochronological constraints. However, these rocks cannot have formed by fractional crystallization from the same parental melt. Buchans-area subvolcanic plutons were exhumed coevally with mineralization and felsic magmatism, preserving a glimpse of the evolution of a hypabyssal system in an ancient volcanic environment. In contrast to the Stewart (1987) model that postulates breccia pipe transport of granitoid cobbles from a sub-volcanic magma chamber to the sea-floor VMS environment, the evidence and comparisons to modern analogues favour exhumation of hypabyssal and plutonic rocks by faulting along caldera or rift walls and (or) erosion. The enigmatic rounding of the granitoid clasts was most likely accomplished in a subaerial or shallow marine environment, and the clasts transported into a VMS-active basin by mass flows (cf. Binney 1987; Stewart 1987). Although the breccia pipe model of Stewart (1987) cannot be completely discounted, it is apparent that it would require very special circumstances to explain the clast morphology and distribution. Conversely, modern volcanic environments demonstrate that the formation of granitoid cobbles can easily be explained solely through sedimentary processes expected for a temporarily emergent volcanic system.

Acknowledgements

This is a contribution to the Geological Survey of Canada Targeted Geoscience Initiative (TGI) 4 (2010–2015). Staff of the Geochronology laboratory assisted in the acquisition of the U–Pb data. Dr. C. van Staal is thanked for a helpful GSC internal review of this manuscript. Drs. T. Grenne, K. Tani, and P. Thurston are also thanked for critical input provided in reviews for the journal.

References

Ainsaar, L., Kaljo, D., Martma, T., Meidla, T., Mannik, P., Nolvak, J., and Tinn, O. 2010. Middle and Upper Ordovician carbon isotope chemostratigraphy in Baltoscandia; a correlation standard and clues to environmental history. Palaeogeography,Palaeoclimatology,Palaeoecology,**294**:189–201.doi:10.1016/j.palaeo.2010.01.003.

Binney, W.P. 1987. A sedimentological investigation of the Maclean channel transported sulfide ores. *In* Buchans Geology, Newfoundland. *Edited by* R.V. Kirkham. Geological Survey of Canada, Paper 86–24, pp. 107–147.

Bostock, H.H. 1988. Geology and petrochemistry of the Ordovician volcanoplutonic Robert's Arm Group, Notre Dame Bay, Newfoundland. Geological Survey of Canada Bulletin 369, Geological Survey of Canada, p 84.

Calon, T.J., and Green, F.K. 1987. Preliminary results of a detailed structural analysis of the Buchans Mine area. *In* Buchans Geology, Newfoundland. *Edited by* R. Kirkham. Geological Survey of Canada, Paper 86–24, pp. 273–288.

Chappell, B.W., and Stephens, W.E. 1988. Origin of infracrustal (I-type) granite magmas. Transactions of the Royal Society of Edinburgh: Earth Sciences, **79**: 71–86. doi:10.1017/S0263593300014139.

Clément, J.P., Legendre, C., Caroff, M., Guillou, H., Cotton, J., Bollinger, C., and Guille, G. 2002. Epiclastic deposits and 'horseshoe-shaped' calderas in Tahiti (Society Islands) and Ua Huka (Marquesas Archipelago), French Polynesia. Journal of Volcanology and Geothermal Research, **120**: 87–101. doi:10.1016/S0377-0273(02)00366-9.

Coombs, A.M., Zagorevski, A., McNicoll, V., and Hanchar, J.M. 2012. Preservation of terranes during the assembly of the Annieopsquotch accretionary tract; inferences from the provenance of a Middle Ordovician ophiolite to arc transition, central Newfoundland Appalachians: Canadian Journal of Earth Sciences, **49**(1): 128–146. doi:10.1139/e11-042.

de Ronde, C.E.J., Baker, E.T., Massoth, G.J., Lupton, J.E., Wright, I.C., Feely, R.A., and Greene, R.R., 2001, Intra-oceanic subduction-related hydrothermal venting, Kermadec volcanic arc, New Zealand: Earth and Planetary Science Letters, v. 193, no. 3-4, pp. 359–369.

de Ronde, C.E.J., Hannington, M.D., Stoffers, P., Wright, I.C., Ditchburn, R.G., Reyes, A.G., Baker, E.T., Massoth, G.J., Lupton, J.E., Walker, S.L., Greene, R.R., Soong, C.W.R., Ishibashi, J., Lebon, G.T., Bray, C.J., and Resing, J.A., 2005,

Evolution of a submarine magmatic-hydrothermal system; Brothers Volcano, southern Kermadec Arc, New Zealand: Economic Geology and the Bulletin of the Society of Economic Geologists, v. 100, no. 6, pp. 1097–1133.

DePaolo, D.J. 1981. Neodymium isotopes in the Colorado Front Range and crust-mantle evolution in the Proterozoic. Nature, **291**: 193–196.

Dunning, G.R., Kean, B.F., Thurlow, J.G., and Swinden, H.S. 1987. Geochronology of the Buchans, Roberts Arm, and Victoria Lake groups and Mansfield Cove Complex, Newfoundland. Canadian Journal of Earth Sciences, **24**(6): 1175–1184. doi:10.1139/e87-113.

Farmin, R. 1937. Hypogene exfoliation in rock masses. Journal of Geology, **45**: 625–635. doi:10.1086/624585.

Frost, B.R., and Frost, C.D. 2008. A geochemical classification for feldspathic igneous rocks. Journal of Petrology, **49**: 1955–1969. doi:10.1093/petrology/egn054.

Frost, B.R., Barnes, C.G., Collins, W.J., Arculus, R.J., Ellis, D.J., and Frost, C.D. 2001. A geochemical classification for granitic rocks. Journal of Petrology, **42**: 2033–2048. doi:10.1093/petrology/42.11.2033.

Graham, I.J., Reyes, A.G., Wright, I.C., Peckett, K.M., Smith, I.E.M., and Arculus, R.J. 2008. Structure and petrology of newly discovered volcanic centers in the northern Kermadec-southern Tofua Arc, South Pacific Ocean. Journal of Geophysical Research, **113**(B8). doi:10.1029/2007JB005453.

Hekinian, R., Muehe, R., Worthington, T.J., and Stoffers, P. 2008. Geology of a submarine volcanic caldera in the Tonga Arc; dive results. Journal of Volcanology and Geothermal Research, **176**: 571–582. doi:10.1016/j.jvolgeores.2008.05.007.

Ishizuka, O., Yuasa, M., and Uto, K. 2002. Evidence of porphyry copper-type hydrothermal activity from a submerged remnant back-arc volcano of the Izu-Bonin Arc; implications for the volcanotectonic history of back-arc seamounts. Earth and Planetary Science Letters, **198**: 381–399. doi:10.1016/S0012-821X(02)00515-0.

Keller, M., and Lehnert, O. 2010. Ordovician paleokarst and quartz sand: Evidence of volcanically triggered extreme climates? Palaeogeography, Palaeoclimatology, Palaeoecology **296**: 297–309. doi:10.1016/j.palaeo.2010.02.015.

Kirkham, R.V., and Thurlow, J.G. 1987. Evaluation of resurgent caldera and aspects of ore deposition and deformation at Buchans. *In* Buchans Geology, Newfoundland. *Edited by* R.V. Kirkham. Geological Survey of Canada, Paper 86–24, pp. 177–194.

Krogh, T.E. 1982. Improved accuracy of U–Pb zircon ages by the creation of more concordant systems using an air abrasion technique. Geochimica et Cosmochimica Acta, **46**: 637–649. doi:10.1016/0016-7037(82)90165-X.

Leat, P.T., Tate, A.J., Tappin, D.R., Day, S.J., and Owen, M.J. 2010. Growth and mass wasting of volcanic centers in the northern South Sandwich Arc, South Atlantic, revealed by new multibeam mapping: Marine Geology, v. 275, no. 1–4, pp. 110–126

Le Friant, A., Harford, C.L., Deplus, C., Boudon, G., Sparks, R.S.J., Herd, R.A., and Komorowski, J.C. 2004. Geomorphological evolution of Montserrat (West Indies); importance of flank collapse and erosional processes. Journal of the Geological Society of London, **161**(1): 147–160. doi:10.1144/0016-764903-017.

Leyrit, H. 2000. Flank collapse and debris avalanche deposits. *In* Volcaniclastic Rocks, from Magmas to Sediments. *Edited by* H. Leyrit and C. Montenat. pp. 111–129.

Lissenberg, C.J., Zagorevski, A., McNicoll, V.J., van Staal, C.R., and Whalen, J.B. 2005. Assembly of the Annieopsquotch accretionary tract, Newfoundland Appalachians; age and geodynamic constraints from syn-kinematic intrusions. Journal of Geology, **113**: 553–570. doi:10.1086/431909.

Ludwig, K.R. 2003. User's manual for Isoplot/Ex rev. 3.00: a Geochronological Toolkit for Microsoft Excel. Special Publication **4**, Berkeley Geochronology Center, Berkeley. p. 70.

Munnecke, A., Calner, M., Harper, D.A.T., and Servais, T. 2010. Ordovician and Silurian sea-water chemistry, sea level, and climate; a synopsis. Palaeogeography, Palaeoclimatology, Palaeoecology, **296**: 389–413. doi:10.1016/j.palaeo.2010.08.001.

Nowlan, G.S., and Thurlow, J.G. 1984. Middle Ordovician conodonts from the Buchans Group, central Newfoundland, and their significance for regional stratigraphy of the Central Volcanic Belt. Canadian Journal of Earth Sciences, **21**(3): 284–296. doi:10.1139/e84-031.

Parrish, R.R., Roddick, J.C., Loveridge, W.D., and Sullivan, R.W. 1987. Uranium-lead analytical techniques at the Geochronology Laboratory, Geological Survey of Canada. Radiogenic age and isotopic studies, Report 1: Geological Survey of Canada, Paper 87–2, pp. 3–7.

Peacock, M.A. 1931. Classification of igneous rock series. Journal of Geology, **39**: 54–67.

Pearce, J.A., Harris, N.B.W., and Tindle, A.G. 1984. Trace element discrimination diagrams for the tectonic interpretation of granitic rocks. Journal of Petrology, **25**: 956–983. doi:10.1093/petrology/25.4.956.

Roddick, J.C. 1987. Generalized numerical error analysis with applications to geochronology and thermodynamics. Geochimica et Cosmochimica Acta, **51**: 2129–2135. doi:10.1016/0016-7037(87)90261-4.

Siebert, L. 1984. Large volcanic debris avalanches: characteristics of source areas, deposits, and associated eruptions. Journal of Volcanology and Geothermal Research, **22**: 163–197. doi:10.1016/0377-0273(84)90002-7.

Sillitoe, R.H. 1985. Ore-related breccias in volcanoplutonic arcs. Economic Geology, **80**: 1467–1514. doi:10.2113/gsecongeo.80.6.1467.

Stern, R.A. 1997. The GSC Sensitive High Resolution Ion Microprobe (SHRIMP): analytical techniques of zircon U-Th-Pb age determinations and performance evaluation. Radiogenic age and isotopic studies, Report 10: Geological Survey of Canada Current Research, **1997-F:** 1–31.

Stern, R.A., and Amelin, Y. 2003. Assessment of errors in SIMS zircon U–Pb geochronology using a natural zircon standard and NIST SRM 610 glass. Chemical Geology, **197**: 111–142. doi:10.1016/S0009-2541(02)00320-0.

Stern, R.J., Tamura, Y., Embley, R.W., Ishizuka, O., Merle, S.G., Basu, N.K., Kawabata, H., and Bloomer, S.H. 2008. Evolution of West Rota Volcano, an extinct submarine volcano in the southern Mariana Arc; evidence from sea floor morphology, remotely operated vehicle observations and (super 40) Ar-(super 39) Ar geochronological studies. Island Arc, **17**: 70–89.

Stewart, P.W. 1983. Granitoid clasts in boulder breccias of McLean Extension orebody, Buchans, Newfoundland. *In* Current Research, Part A, Geological Survey of Canada, Paper 83-1A, pp. 321–324.

Stewart, P.W. 1984. Geochemistry of granitoid clasts from McLean Extension orebody, Buchans, Newfoundland, and implications on their possible source. *In* Current Research, Part A, Geological Survey of Canada, Paper 84-1A, pp. 467–472.

Stewart, P.W. 1985. Geology, geochemistry, geochronology and genesis of granitoid clasts in breccia-conglomerates, McLean Extension orebody, Buchans, Newfoundland. Unpublished MSc. Thesis, Memorial University of Newfoundland, p. 327.

Stewart, P.W. 1987. Geology and genesis of granitoid clasts in the McLean Extension transported orebody. *In* Buchans Geology, Newfoundland. *Edited by* R. Kirkham. Geological Survey of Canada, Paper 86-24, pp. 149–176.

Stoffers, P., Worthington, T.J., Schwarz-Schampera, U., Hannington, M.D., Massoth, G.J., Hekinian, R., Schmidt, M., Lundsten, L.J., Evans, L.J., Vaiomo'unga, R., and Kerby, T. 2006. Submarine volcanoes and high-temperature hydrothermal venting on the Tonga Arc, Southwest Pacific. Geology, **34**: 453–456. doi:10.1130/G22227.1.

Streckeisen, A.L., and Le Maitre, R.W. 1979. A chemical approximation to the modal QAPF classification of the igneous rocks. Neues Jahrbuch für Mineralogie, Abhandlungen, **136**: 169–206.

Swinden, H.S., Jenner, G.A., and Szybinski, Z.A. 1997. Magmatic and tectonic evolution of the Cambrian-Ordovician Laurentian margin of Iapetus; geochemical and isotopic constraints from the Notre Dame Subzone, Newfoundland. Geological Society of America Memoir, **191**: 337–365.

Tămaş, C., and Milési, J.P. 2002. Hydrovolcanic Breccia Pipe Structures - General Features and Genetic Criteria. I. Phreatomagmatic Breccias. Studia UBB Geologia, **47**: 127–147.

Tani, K., Fiske, R.S., Tamura, Y., Kido, Y., Naka, J., Shukuno, H., and Takeuchi, R. 2008. Sumisu Volcano, Izu-Bonin arc, Japan; site of a silicic caldera-forming eruption from a small open-ocean island. Bulletin of Volcanology, **70**: 547–562. doi:10.1007/s00445-007-0153-2.

Tarney, J., and Jones, C.E. 1994. Trace element geochemistry of orogenic igneous rocks and crustal growth models, Journal of the Geological Society, London, **151**: 855–868.

Taylor, R. 2009. Ore textures: Recognition and Interpretation. Springer. 288 p.

Taylor, S.R., and McLennan, S.M. 1985. The Continental Crust: Its Composition and Evolution. Blackwell, Oxford, U.K.

Thurlow, J.G. 1977. Occurrence, origin and significance of mechanically transported sulphide ores at Buchans, Newfoundland. *In* Volanic Processes in Ore Genesis. Geological Society of London, Special Publication 7. p. 127.

Thurlow, J.G. 1981*a*. Geology, ore deposits and applied rock geochemistry of the Buchans Group, Newfoundland, unpublished Ph.D. thesis, Memorial University of Newfoundland, p. 305.

Thurlow, J.G. 1981*b*. The Buchans Group: its stratigraphic and structural setting. *In* The Buchans Orebodies: Fifty Years of Geology and Mining, *Edited by* E.A. Swanson, D.F. Strong, and J.G. Thurlow. Geological Association of Canada, Special Paper 22. pp. 79–90.

Thurlow, J.G. 2001. Geology of the Buchans orebodies - a 1999 summary. *In* Evans, D. and Kerr, A. (eds.) Geology and mineral deposits of the northern Dunnage Zone, Newfoundland Appalachians. Geological Association of Canada - Mineralogical Association of Canada Joint Annual Meeting, St. John's, Newfoundland, Field Trip Guide Book A2, pp. 155–163.

Thurlow, J.G, and Swanson, E.A. 1981. Geology and ore deposits of the Buchans area, central Newfoundland. *In:* The Buchans Orebodies: Fifty Years of Geology and Mining. *Edited by* E.A. Swanson, D.F. Strong and J.G. Thurlow. Geological Association of Canada, Special Paper 22. pp. 113-142.

Thurlow, J.G., and Swanson, E.A. 1987. Stratigraphy and structure of the Buchans Group. *In* Buchans Geology, Newfoundland. *Edited by* R.V. Kirkham. Geological Survey of Canada, Paper 86-24, pp. 35–46.

van Hees, G.W.H, 2011. Chemostratigraphy and alteration geochemistry of the Lundberg and Engine House volcanogenic massive sulphide mineralization, Buchans, Central Newfoundland. M.Sc. thesis, University of Ottawa.

van Hees, G., Zagorevski, A., and Hannington, M. 2012. Volcanology and Stratigraphy of the Lundberg Zone, Buchans, Newfoundland. Current Research (2012), Newfoundland Department of Mines and Energy Geological Survey, Report 12-1.

van Kranendonk, M.J., Bleeker, W., and Ketchum, J. 2006. Phreatomagmatic boulder conglomerates at the tip of the ca 2772 Ma Black Range dolerite dyke, Pilbara Craton, Western Australia. Australian Journal of Earth Sciences, **53**: 617–630. doi:10.1080/08120090600686777.

van Staal, C.R., Dewey, J.F., Mac Niocaill, C., and McKerrow, W.S. 1998. The Cambrian-Silurian tectonic evolution of the Northern Appalachians and British Caledonides; history of a complex, west and southwest Pacific-type segment of Iapetus. *In* Lyell: the Past is the Key to the Present. *Edited by* D.J. Blundell and A.C. Scott. Geological Society, London. pp. 199–242.

van Staal, C.R., Whalen, J.B., McNicoll, V.J., Pehrsson, S., Lissenberg, C.J., Zagorevski, A., van Breemen, O., and Jenner, G.A. 2007. The Notre Dame Arc and the Taconic Orogeny in Newfoundland. *In* 4-D Framework of continental crust. *Edited by* R.D. Hatcher, Jr., M.P. Carlson, J.H. McBride, and J.R. Martinez Catalan. Geological Society of America. pp. 511–552.

Videt, B., Paris, F., Rubino, J.-L., Boumendjel, K., Dabard, M.-P., Loi, A., Ghienne, J.-F., Marante, A., and Gorini, A. 2010. Biostratigraphical calibration of third order Ordovician sequences on the northern Gondwana platform. Palaeogeography, Palaeoclimatology, Palaeoecology, **296**: 359–375. doi:10.1016/j.palaeo.2010.03.050.

Whalen, J.B. 1985. Geochemistry of an island-arc plutonic suite: the Uasilau-Yau Yau intrusive complex, New Britain, P.N.G. Journal of Petrology, **26**: 603–632.

Whalen, J.B. 2012. Geochemical and isotopic (Nd, O, Pb and Sr) data from igneous rocks of the Notre Dame subzone and adjacent tectonostratigraphic zones, western and central Newfoundland. Geological Survey of Canada, Open File 7202. doi:10.4095/291593..

Whalen, J.B., and Frost, C.D. 2013. The Q-ANOR diagram: A tool for the petrogenetic and tectonmagmatic characterization of granitic suites. South-Central Section, Geological Society of America, Austin, Texas, abstract.

Whalen, J.B, Jenner, G.A., Longstaffe, F.J, Gariépy, C., and Fryer, B.J. 1997. Implications of granitoid geochemical and isotopic (Nd, O, Pb) data from the Cambrian-Ordovician Notre Dame arc for the evolution of the Central Mobile belt, Newfoundland Appalachians. *In* The Nature of Magmatism in the Appalachian Orogen. *Edited by* K. Sinha, J.B. Whalen, and J.P. Hogan. Geological Society of America, Memoir **191**: 367–395

Whalen, J.B., McNicoll, V.J., van Staal, C.R., Lissenberg, C.J., Longstaffe, F.J., Jenner, G.A., and van Breemen, O. 2006. Spatial, temporal and geochemical characteristics of Silurian collision-zone magmatism: an example of a rapidly evolving magmatic system related to slab break-off. Lithos, **89**: 377–404. doi:10.1016/j.lithos.2005.12.011.

White, A.J.R., and Chappell, B.W. 1988. Some supracrustal (S-type) granites of the Lachlan Fold Belt. Transactions of the Royal Society of Edinburgh, **79**: 169–181. doi:10.1017/S026359330001419X.

Zagorevski, A., and Rogers, N. 2008. Stratigraphy and structural geology of the Ordovician volcano-sedimentary rocks in the Mary March Brook area. Current Research (2008) Newfoundland Department of Mines and Energy Geological Survey, Report 08-01, pp. 111–123.

Zagorevski, A., and Rogers, N. 2009. Geochemical characteristics of the Ordovician volcano-sedimentary rocks in the Mary March Brook area. Current Research (2009) Newfoundland Department of Mines and Energy Geological Survey, Report 09-01, pp. 271–288.

Zagorevski, A., and Rogers, N. 2011. Geochemical Data of the Buchans-Robert's Arm Belt and adjacent units in central Newfoundland and Notre Dame Bay regions, Geological Survey of Canada, Open File 6728, 1CD-ROM.

Zagorevski, A., and van Staal, C.R. 2011. The Record of Ordovician Arc-Arc and Arc-Continent Collisions in the Canadian Appalachians During the Closure of Iapetus, *in* Brown, D., and Ryan, P.D., eds., Arc-Continent Collision, Frontiers in Earth Sciences: Berlin Heidelberg, Springer-Verlag. pp. 341–371.

Zagorevski, A., Rogers, N., McNicoll, V., Lissenberg, C.J., van Staal, C.R., and Valverde-Vaquero, P. 2006. Lower to Middle Ordovician evolution of peri-Laurentian arc and back-arc complexes in the Iapetus: Constrains from the Annieopsquotch Accretionary Tract, central Newfoundland. Geological Society of America Bulletin, **118**: 324–342. doi:10.1130/B25775.1.

Zagorevski, A., McNicoll, V., and van Staal, C.R. 2007*a*. Distinct Taconic, Salinic and Acadian deformation along the Iapetus suture zone, Newfoundland Appalachians. Canadian Journal of Earth Sciences, **44**(11): 1567–1585. doi:10.1139/E07–037.

Zagorevski, A., McNicoll, V.J., van Staal, C.R., and Rogers, N. 2007*b*. Tectonic history of the Buchans Group; evidence for late Taconic accretion of a peri-Laurentian arc terrane and its reimbrication during the Salinic Orogeny. Abstracts with Programs - Geological Society of America **39**(1): 51.

Zagorevski, A., Lissenberg, C.J., and van Staal, C.R. 2009. Dynamics of accretion of arc and backarc crust to continental margins: Inferences from the Annieopsquotch Accretionary Tract, Newfoundland Appalachians. Tectonophysics, **479**: 150–154. doi:10.1016/j.tecto.2008.12.002.

Zagorevski, A., Rogers, N., and Haslam, R. 2010. Geology and significance of the Harry's River mafic volcanic rocks, Buchans area, Newfoundland: Current Research (2010) Newfoundland Department of Mines and Energy Geological Survey, Report 10–1, pp. 373–384.

Appendix A: U–Pb zircon analytical techniques

Heavy mineral concentrates were prepared from the samples using standard mineral separation techniques, including crushing, grinding, hydrogravimetric Wilfley table separation, and heavy liquid separation. This process was followed by final separation of the zircon grains by magnetic susceptibility using a Frantz isodynamic separator and hand picking using a binocular microscope.

U–Pb ID–TIMS techniques utilized in this study are modified after Parrish et al. (1987), with treatment of analytical errors after Roddick (1987). All of the zircon fractions were abraded following the technique of Krogh (1982). U–Pb ID–TIMS analytical results are presented in Table 2 and displayed in a concordia plot (Fig. 2*a*). All ages uncertainties are presented at the 2σ level.

SHRIMP II analyses were conducted using analytical procedures described by Stern (1997), with standards and U–Pb calibration methods following Stern and Amelin (2003). Zircons from the samples and fragments of the GSC laboratory zircon standard (z6266 zircon, with $^{206}Pb/^{238}U$ age = 559 Ma) and a secondary zircon standard (Temora 2) were cast in an epoxy grain mount (see Table 3 for GSC mount number), polished with diamond compound to reveal the grain centres, and photographed in transmitted light. Internal features of the zircons (such as zoning, structures, alteration, etc.) were characterized in back-scattered electron (BSE) and cathodoluminescence (CL) modes utilizing a Zeiss Evo 50 scanning electron microscope (SEM). Mount surfaces were evaporatively coated with 10 nm of high-purity Au. Analyses were conducted using an O^- primary beam, projected onto the zircons with an elliptical spot (17 μm × 23 μm). The count rates of ten masses including background were sequentially measured over five scans with a single electron multiplier and a pulse-counting system with dead-time of 23 ns. Offline data processing was accomplished using customized in-house software. The SHRIMP analytical data are presented in Table 3, where the 1σ external errors of $^{206}Pb/^{238}U$ ratios reported in the data table incorporate a 1.0%–1.1% error in calibrating the standard zircon (Stern and Amelin 2003). No fractionation correction was applied to the Pb-isotope data; common Pb correction utilized the Pb composition of the surface blank (Stern 1997). The data are plotted in concordia diagrams with errors at the 2σ level (Figs. 2*b*, 2*c*), using Isoplot v. 3.0 (Ludwig 2003) to generate the plots and calculate the weighted averages.